

1 Global tropical cyclone size and intensity reconstruction dataset for 2 1959–2022 based on IBTrACS and ERA5 data

3 Zhiqi Xu¹, Jianping Guo^{2*}, Guwei Zhang¹, Yuchen Ye³, Haikun Zhao³, Haishan Chen³

4 ¹Institute of Urban Meteorology, China Meteorological Administration, Beijing 100089, China

5 ²State Key Laboratory of Severe Weather, Chinese Academy of Meteorological Sciences, Beijing 100081, China

6 ³Key Laboratory of Meteorological Disaster, Ministry of Education (KLME)/Joint International Research Laboratory of
7 Climate and Environment Change (ILCEC)/Collaborative Innovation Center on Forecast and Evaluation of Meteorological
8 Disasters (CIC-FEMD), Nanjing University of Information Science and Technology, Nanjing, 210044, China

9 **Correspondence:** J. Guo (Email: jpguocams@gmail.com)

10 **Abstract.** Tropical cyclones (TCs) are powerful weather systems that can cause extreme disasters. ~~We extensively utilize The~~
11 ~~The~~ International Best Track Archive for Climate Stewardship (IBTrACS) dataset ~~provides the extensively accessed widely~~
12 ~~used data has beenareis used extensively~~ to estimate TC climatology. However, it has low data coverage, lacking intensity and
13 outer size data for more than half of all recorded storms, and is therefore insufficient as a reference for researchers and decision
14 makers. To fill this data gap, we reconstructed a long-term TC dataset by integrating IBTrACS and European Centre for
15 Medium-Range Weather Forecasts Reanalysis 5 (ERA5) data. This ~~reconstructednew~~ dataset covers the period 1959–2022,
16 with 3 h temporal resolution. Compared to the IBTrACS dataset, it contains approximately 3–4 times more data points per
17 characteristic. We established machine learning models to estimate the maximum sustained wind speed (V_{max}) and radius ~~to~~
18 ~~of~~ maximum wind ~~speed~~ (R_{max}) in six basins for which TCs ~~were are~~ generated, using ERA5-derived 10 m azimuthal ~~median~~
19 ~~mean~~ azimuthal wind profiles as input, with V_{max} and R_{max} data from the IBTrACS dataset used as ~~learning targettraining~~
20 data. ~~Furthermore, we employ An an~~ empirical wind–pressure relationship and six wind profile models ~~were are employed~~ to
21 estimate the minimum central pressure (P_{min}) and outer size of the TCs, respectively. Overall, this high-resolution TC
22 reconstruction dataset demonstrates ~~sd~~ global consistency with observations, exhibiting mean biases of <1% for V_{max} and 3%
23 for R_{max} and P_{min} in almost all basins. The ~~new~~ dataset is publicly available from [https://doi.org/](https://doi.org/10.5281/zenodo.13919874)
24 ~~10.5281/zenodo.13919874~~ ~~10.5281/zenodo.12740372~~ (Xu et al., 2024) and ~~substantialsignificantly~~ advances our
25 understanding of TC climatology, thereby facilitating risk assessments and defenses against TC-related disasters.

26 1. Introduction

27 Tropical cyclones (TCs) are ~~powerful~~~~formidable~~ weather systems accompanied by gale winds, ~~torrential~~~~heavy~~ rainstorms,
28 ~~substantial~~~~significant~~ waves, and ~~devastating~~~~severe~~ storm surges, which cause extensive damage in affected regions (Gray,
29 1968). ~~During the 2003-2022 period, the global average of tropical cyclone~~~~TCs was~~ 104 annually, resulting in estimated
30 ~~annual economic losses of 95.6 billion US dollars and affecting over~~~~more than 3.2 million individuals~~~~people~~ ~~During the past~~
31 ~~two decades, TCs have resulted in an average annual economic loss of 29 billion~~ ~~US dollars, affecting more than 22 million~~
32 ~~individuals~~ (Guha-Sapir ~~CRED, 2017~~2023; Geiger et al., 2018). Given the considerable scale and frequency of TC-related
33 disasters, a comprehensive understanding of TC climatology is essential for effective risk assessment, emergency planning,
34 and community resilience enhancement.

35 TCs are typically characterized according to their intensity, size, location, and translation speed (Weber et al., 2014).
36 Many studies have reported increasing TC intensity at both the basin and global scales under global warming (e.g., Webster et
37 al., 2006; Gualdi et al., 2008; Wu et al., 2022). Vincent et al. (2014) ~~detect~~~~detects~~~~eded~~ a 30% increase in high-intensity TCs at
38 the global scale. Mei and Xie (2016) ~~demonstrat~~~~demonstrated~~~~eded~~ a significant correlation between TC intensification and
39 increasing sea surface temperatures (SSTs) in East and Southeast Asia. In addition, Walsh et al. (2016) observe~~d~~ significant
40 increasing trends in TC intensity ~~have been~~~~observed~~ in the Atlantic basin over the past few decades ~~(Walsh et al., 2016)~~.
41 However, assessments of the response of TC intensity to climate change are subject to uncertainty, partly due to the challenging
42 and costly process of collecting observational al data (Gualdi et al., 2008; Knutson et al., 2019). Furthermore, the size of TCs
43 may~~movement of TCs may be~~ significantly influenced ~~_~~~~by~~ their size~~movement~~ (Liu and Chan, 1999), further contributing to
44 their destructive potential (Xu et al., 2020). Similarly, a significant increase in TC size ~~was~~~~isis~~~~was reported to be~~ proportional
45 to surface latent heat flux under warmer air and ocean temperatures (Hill and Lackmann, 2009; Radu et al., 2014). Xu et al.
46 (2020) demonstrates~~sde~~ that TC size increases with ocean warming, based on idealized experiments. Sun et al. (2013, 2014)
47 ~~discover~~~~discovers~~~~eded~~ that TC size increases significantly as SST increases through a modeling analysis. However, the

48 conclusions of these case studies are necessarily limited, and the relationships between TC size and climatology factors remain
49 unclear due to the lack of historical records (Xu et al., 2020).

50 The International Best Track Archive for Climate Stewardship (IBTrACS) dataset is one of the most commonly used
51 sources for TC data; it contains location, intensity, and size data for all known tropical and subtropical cyclones at a resolution
52 of 3 h (Knapp et al., 2010). ~~In t~~This dataset ~~utilizes~~ maximum sustained wind speed (V_{max}) and minimum central pressure
53 (P_{min}) ~~are used~~ to quantify TC intensity (Simpson, 1974; Chavas et al., 2017; Casas et al., 2023). Among the several metrics
54 that ~~have been~~ ~~are~~ defined to measure TC size, one of the most widely recognized is the radius ~~of t~~ maximum wind ~~speed~~
55 (R_{max} , Chavas et al., 2015; Ren et al., 2022). Radial distances from the cyclone center to locations where sustained wind
56 speeds of 34, 50 and 64 knots (~17, 26, and 33 m/s) are observed ~~near the en~~ surface, i.e., R_{34} , R_{50} , and R_{64} , are also ~~widely~~
57 used ~~metrics~~ to estimate TC size (Pérez-Alarcón et al., ~~2023~~2021). However, reliable TC size and intensity estimates are
58 available only from 1988 onwards (Demuth et al., 2006), and post-storm analyses of wind radii, including R_{34} , R_{50} , and R_{64} ,
59 ~~did do not~~ ~~have only~~ commenced ~~until~~ ~~since~~ 2004 (Gori et al., 2023). Furthermore, more than half of all recorded storms lack
60 intensity and size data, often with only location data provided even during periods when post-storm analyses ~~were~~ ~~are~~ ~~were~~ ~~are~~
61 conducted. Thus, constructing a TC climatology is an arduous task due to low data coverage.

62 ~~Previous researches have extensively~~ ~~widely~~ used ~~Machine-machine~~ learning ~~has been~~ ~~is~~ ~~widely~~ ~~used~~ to reconstruct TC
63 datasets. Yang et al. (2022) ~~divide~~ ~~d~~ hurricane wind fields into symmetric and asymmetric components, and propose ~~d~~ a
64 downscaling model based on the XGBoost software library to reconstruct TC structure; however, V_{max} and R_{max} ~~were~~
65 ~~are~~ ~~were~~ ~~are~~ the model input variables. Zhuo and Tan (2023) ~~applied~~ ~~s~~ ~~ied~~ deep learning algorithms to estimate reliable TC sizes
66 over the western North Pacific during 1981–2017, based on a homogeneous satellite database. Li et al. (2024) propose ~~d~~ a
67 transfer learning-based generative adversarial network framework to derive TC wind fields from synthetic aperture radar
68 images. Eusebi et al. (2024) demonstrate ~~d~~ ~~s~~ that a physics-informed neural network can produce accurate reconstructions of
69 TC wind and pressure fields by assimilating observations in a computationally efficient manner. Nevertheless, the datasets

70 used in these studies ~~were we~~are generally limited to several cases or specific regions of interest, and some are not publicly
71 available.

72 By contrast, reanalysis datasets such as the fifth-generation European Centre for Medium-Range Weather Forecasts
73 (ECMWF) Reanalysis 5 (ERA5) dataset (Hersbach et al., 2020), the 55-year Japanese Reanalysis (Kobayashi et al., 2015), and
74 US National Centers for Environmental Prediction and National Centre for Atmospheric Research Reanalysis products (Kistler
75 et al., 2001), which combine past observations and model results through data assimilation, have unique advantages in terms
76 of data availability and spatiotemporal coverage. ~~Schenkel et al. (2017) evaluated whether reanalysis dataset can be used to~~
77 ~~derive a long-term TC size dataset utiliz~~ing QuikSCAT ~~D~~data. Zick and Matyas (2016) explored the impact of satellite-
78 ~~derived precipitation over ocean on TC in the North American Regional Reanalysis. Gori et al. (2023) utilize~~s ERA5
79 ~~reanalysis data to estimate the TC outer size, and a physics-based TC-wind model to estimate the radius of maximum wind.~~
80 ~~Thompson et al. (2024) constructed details the creation of a tropical cyclone (TC) size dataset using the NCEP/NCAR~~
81 ~~Reanalysis I dataset for landfalling TCs along the United States coastline from 1948 to 2022.~~ Previous studies ~~have have~~
82 ~~suggeste~~d that ERA5 products are among the most promising reanalysis data sources in terms of representing TC outer size
83 and structure, due to their relatively fine horizontal grid spacing (Bian et al., 2021; Pérez-Alarcón et al., ~~2023~~2021; Dulac et
84 al., 2024). ~~Yeasmin et al. (2023) demonstrate~~s that ~~t~~he reconstruction of TC proxies using ERA5 ~~data has been~~are
85 ~~demonstrated to be~~wasis a viable approach ~~(Yeasmin et al., 2023)~~. Nevertheless, due to horizontal resolution limits and
86 conservative physics parameterizations, reanalysis products have exhibited large underestimation and overestimation of TC
87 V_{max} and R_{max} values, respectively (Hatsushika et al., 2006; Schenkel and Hart, 2012). Thus, despite the substantial body
88 of research reconstructing the outer sizes and proxies of TCs using ERA5 data (Bian et al., 2021; Gori et al., 2023; Pérez-
89 Alarcón et al., ~~2023~~2021), studies ~~that have employed this data to derive based on its it to derive~~relatively accurate TC
90 intensity data are lacking.

91 In this study, we exploit~~ed~~ the advantages of the IBTrACS and ERA5 datasets to generate a ~~reconstructed~~new TC dataset
92 containing all characteristics of TCs. Given the high degree of accuracy demonstrated by the ERA5 data in capturing TC

93 structures, we employed ERA5-derived azimuthal ~~median–mean~~ azimuthal wind profiles in conjunction with a machine
94 learning model to reduce the bias observed in the V_{max} and R_{max} of TCs between the ERA5 and IBTrACS datasets. In
95 addition, we modeled six TC radial wind profiles to compute R_{34} , R_{50} , and R_{64} . The resulting long-term TC reconstruction
96 dataset covering the period 1959–2022 is anticipated to facilitate future TC climatology research. The generated dataset is
97 approximately 3–4 times larger than the IBTrACS dataset in terms of the number of records per characteristic.

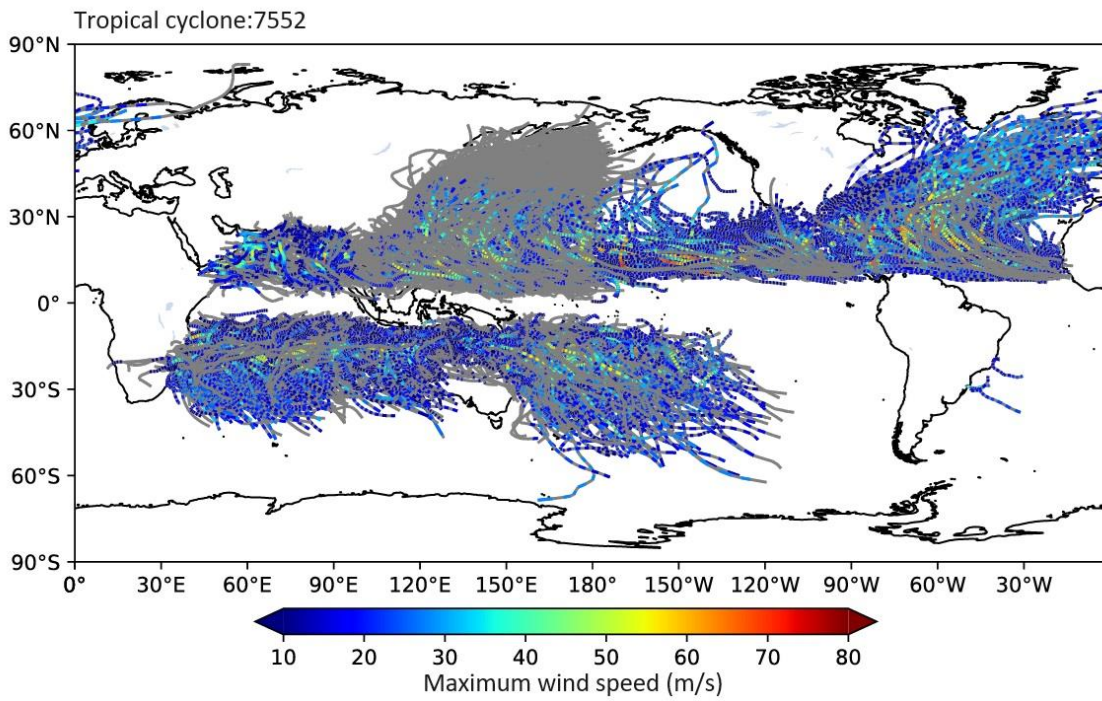
98 In the subsequent sections, we describe the IBTrACS and ERA5 datasets and the methodology used to create the novel
99 TC reconstruction dataset. ~~We report and discuss t~~~~he findings are reported and discussed~~ in comparison with IBTrACS data
100 according to a comprehensive set of statistical metrics. Finally, we consider the potential applications of the reconstructed TC
101 dataset.

102 2. Data

103 2.1 IBTrACS data

104 ~~We obtain Data data~~ on TC tracks, intensity, and size ~~were are obtained~~ from the IBTrACS (version 4r01 [in netCDF format](#)),
105 which is a unified dataset containing track estimates for all TC basins with a 3 h temporal resolution, based on data produced
106 by tropical warning centers. As the TC R_{max} data from all main TC basins ~~were are~~ accessible from U.S. agencies ([the
107 National Oceanic and Atmospheric Administration’s \(NOAA\) National Hurricane Center \(NHC\) for the North Atlantic and
108 east Pacific and the military’s Joint Typhoon Warning Center \(JTWC\) for the remainder of the globe](#)), we employed these data
109 and ~~excluded–exclude~~ the irregular time steps. ~~We use a~~All TC events in all basins ~~were are used~~, except for those over the
110 South Atlantic, where TC generation is insufficient. A comprehensive overview of the recorded TC characteristics is presented
111 in Table 1. The IBTrACS dataset encompasses a total of 7,552 TCs on a global scale, spanning the period 1959–2022,
112 corresponding to 423,296 individual time points. However, [IBTrACS dataset](#) only ~~record~~~~records~~ 125,477 V_{max} , 142,430 P_{min} ,
113 and 94,415 R_{max} values ~~were are recorded~~. TC tracks and V_{max} data extracted from the IBTrACS dataset are presented in

114 Fig. 1.



115
116
117
118

Figure 1: Overview of the tracks and 10-m maximum wind speeds of tropical cyclones in IBTrACS dataset. Grey lines represent the unrecorded wind speeds.

Table 1: Basic information on the number of recorded tropical cyclone characteristics from 1959 to 2022 recorded in IBTrACS.

Basin	Time point	V_{max}	P_{min}	R_{max}	R_{34}	R_{50}	R_{64}
Western Pacific	152362	26604	61018	28715	19340	10641	7149
North Atlantic	55679	28310	21409	18161	14961	7630	4212
North Indian	24101	5481	5476	4281	2354	1029	614
South Indian	86790	23935	24468	16367	10697	5108	2977
South Pacific	45189	12322	12467	7169	4827	2577	1521
Eastern Pacific	59175	28825	17592	19722	12283	6482	3986
Global	423296	125477	142430	94415	64462	33467	20459

122 2.2 ERA5 data

ERA5 is the latest ECMWF reanalysis, following a decade of developments in model physics, core dynamics, and data

assimilation (Hersbach et al., 2020). We utilized the main ERA5 dataset for the period 1959–2022 to estimate the track,

intensity, and size of each TC. The spatial resolution of the ERA5 dataset is $0.25^\circ \times 0.25^\circ$, with a temporal resolution of 3 h,

aligning with that of the IBTrACS dataset. ~~We exclude pPre-1959 ERA5 back-extension data were are not adopted.~~

TCs in these data ~~exhibiteexhibite~~ unrealistically high levels of tension (Bell, 2021). Notably, despite the higher uncertainty

associated with TC intensity data derived from ERA5 for the pre-satellite time period (1959–1978), comparisons of TC

intensity pre- and post-1979 revealed similar climatological distributions for both TC groups in all basins (Fig. S1). We

employed 10 m surface meridional and latitudinal wind speeds to obtain 10 m azimuthal–mean azimuthal wind profiles for

TCs. ~~We utilize tThe sea level pressure (SLP) was is utilized~~ to provide environmental pressure data for computing the TC

central pressure. ~~We derive the pParameters~~ including the SLP; relative vorticity at 700, 850, and 925 hPa; and geopotential

height at 700 and 850 hPa ~~were are derived~~ from the ERA5 data to identify TC centers.

3. Methodology

3.1 TC center identification and azimuthal wind profile estimation

136 ~~We identify~~ TC centers in the ERA5 data, ~~were are identified~~ based on the method of Schenkel [et al. \(2017\)](#). ~~We initially~~
137 ~~ascertain~~ ~~the~~ position of each TC within the reanalysis grid ~~was is initially ascertained~~ utilizing the IBTrACS position
138 as a first guess. To remove uncertainties associated with TC centers in the reanalysis data, ~~we obtain~~ the ~~centroids~~ ~~centers~~ of
139 six reanalysis variables (SLP; relative vorticity at 700, 850, and 925 hPa; and geopotential height at 700 and 850 hPa) ~~by~~
140 ~~calculating~~ ~~computing~~ the ~~center of mass~~ ~~centroids~~ ~~maximum~~ of positive relative vorticity values and ~~minimum of negative~~
141 ~~values of other variables~~ values over the grid near the first guess position ($\pm 2^\circ$) using ~~p~~Python v3.10.7. Subsequently, ~~we~~
142 ~~average~~ ~~Then the center~~ ~~centroids~~ ~~was are~~ averaged over the grid near the first guess position to adjust the position of the
143 estimated reanalysis TC center.

144 ~~We estimate a~~ Azimuthal wind profiles based on the ERA5 data, ~~were are estimated~~ as described by Chavas and Vigh
145 (2014). First, ~~we subtract~~ estimated environment wind fields, which ~~were are~~ calculated as 0.55 of the TC translation vectors
146 rotated 20° counterclockwise (Lin and Chavas, 2012), ~~were are subtracted~~ from the meridional and latitudinal wind speeds.
147 ~~We determine~~ TC translation vectors ~~were are determined~~ according to the TC positions at the next and current time points in
148 the IBTrACS data. Next, ~~we interpolate~~ the 10 m surface meridional and latitudinal wind fields ~~were are interpolated~~ to a TC-
149 centered polar coordinate. In contrast to the method of Chavas and Vigh, we ~~did do~~ not exclude grid points over land to obtain
150 the TC intensity after landfall. Then, ~~we employ~~ the parameter \mathcal{X} , defined as the normalized average magnitude of all vectors
151 from the TC center to each grid point included at a specified radius (Chavas and Vigh, 2014) ~~was is employed~~ to remove
152 asymmetrical radial bins by excluding radial bins with $\mathcal{X} > 0.5$. Finally, ~~we calculate~~ the TC 10 m azimuthal–mean azimuthal
153 wind profiles ~~were are calculated~~ as changes in wind speed with distance from the TC center, with grid points spaced at 10 km
154 intervals. ~~We obtain~~ ~~the~~ ERA5-derived TC V_{max} (V_{max_ERA5}) and R_{max} (R_{max_ERA5}) ~~were are obtained~~ from the wind
155 profiles.

156 3.2 Machine learning model for reconstructing TC V_{max} and R_{max} from ERA5 data

157 As shown in Fig. 2, there ~~were are~~ discernible biases in all six TC basins between the ERA5- and IBTrACS-derived V_{max} and
158 R_{max} values. The biases of V_{max} ~~were are~~ less dependent on the basin, suggesting the systematic underestimation of V_{max}

159 by the ERA5 data, partly due to the lower P_{min} and the underestimation of the TC wind-pressure relation described in ERA5
160 (Magnusson et al., 2021). Besides, ~~Moreover,~~ convective-scale processes substantially influence V_{max} , which ~~is~~
161 ~~significantly~~ substantially influenced by convective scale processes that are ~~not~~ cannot be adequately represented in global
162 models, leading to an inherent tendency for underestimation is largely dependent on convective scale ($O(1\text{ km})$) processes that
163 ~~are not resolved in the global models, and it is therefore expected to be regularly underestimated.~~ To further demonstrate the
164 performance of ERA5-derived data, we select the Saffir-Simpson categories as the uniform scale for all the basins, and analyze
165 the differences between ERA5-derived and observed data across various wind speed ranges, following the methods in previous
166 researches (Wright, 2019; Bloemendaal et al., 2022; Mo et al., 2023). In contrast, biases ~~were~~ are more pronounced for larger
167 V_{max} values, with underestimation detected for wind speeds exceeding 20 and 30 m/s for Saffir-Simpson categories 1–2 and
168 3–5, respectively, in all six basins. Notably, this bias even exceeded ~~sed~~ 40 m/s for Saffir-Simpson categories 3–5 in the East
169 Pacific basin. In addition, ERA5-derived results overestimated R_{max} by >15 km in all basins, and by >80 km in the West
170 Pacific (WP) basin. The large biases produced by ERA5 motivated us to establish a ~~reconstructed~~ new TC dataset that is more
171 consistent with observations.

172 Previous studies have indicated that despite the ~~discrepancy~~ modesty of ERA5 derived TC intensity data, the ERA5
173 dataset accurately depicts TC structural alterations (Bian et al., 2021). Therefore, we used the TC 10-m azimuthal mean
174 azimuthal wind speed at radial distances from 0 to 1000 km, at 10 km intervals, as a parameter to estimate V_{max} in each
175 basin. The parameters also included the TC translation speed, given that the IBTrACS V_{max} data (V_{max-IB}) represent a
176 combination of the environmental and TC wind fields. After testing ~~s~~ A series of ~~Several~~ machine learning models were
177 ~~tested within~~ using python v3.10.7, including ~~ann~~ random forest (RF) algorithms, artificial neural network (ANN),
178 convolutional neural network, support vector regressor, and multivariate linear regression (Table 2 and 3) ~~multilayer~~
179 ~~perceptron regression.~~ For a detailed account of the hyperparameter selections for each model, please refer to the
180 ~~supplementary materials. Is,~~ Although the ANN derived R_{max} R_{max} obtained by ANN exhibited a stronger
181 ~~correlations with observations, the root mean square error (RMSE) of V_{max} the R_{max} and R_{max} deriv~~ obtained by RF

with observations were considerably smaller than those obtained derived by other models and random forest (RF) algorithms, we found that Therefore, we found that RF provided the most robust predictions. For a comprehensive detailed account of the hyperparameter calibration determination selections process and a comparative analysis of the model performance of for each machine learning models, please refer to the supplementary materials. A detailed description of the determination of the expression hyperparameters and comparison of the performance for the function Feach model can be found in the Supplementary materials. Therefore, as evidenced by higher correlations and smaller root mean square error RMSEs (RMSE) values in most basins. Accordingly, Therefore, and an RF regressor was developed to predict reconstructed V_{max} (V_{max_RC}), as follows:

$$V_{max_RC} = RF(V_0, V_{10}, V_{20}, \dots, V_{1000}, V_{TS}) \quad (1)$$

where RF and V_{TS} are the RF regressor and TC translation speed, respectively, and $V_0, V_{10}, V_{20}, \dots, V_{1000}$ refer to the 10 m azimuthal mean azimuthal wind speeds at radial distances from 0 to 1000 km.

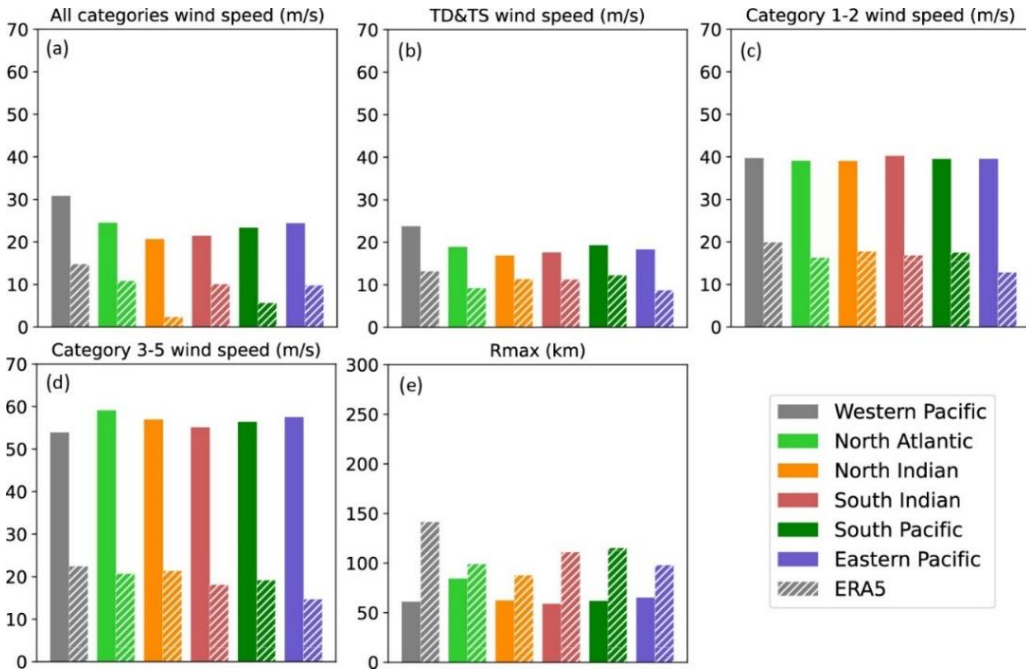


Figure 2: Bar charts for comparing the mean value of the 10-m maximum wind speeds and the radii to maximum winds. Each of the colors indicates a different basin. Solid and dashed bars represent IBTrACS and ERA5-derived data.

Despite the discrepancy in TC intensity, Bian et al. (2021) demonstrates that ERA-5 accurately depicts TC structural alterations. Previous studies have indicated that despite the discrepancy of ERA5 derived TC intensity data, the ERA5 dataset accurately depicts TC structural alterations (Bian et al., 2021). Therefore, we used the TC 10 m azimuthal-mean azimuthal

wind speed at radial distances from 0 to 1000 km, at 10 km intervals, as a parameter to estimate V_{max} in each basin. The parameters also included the TC translation speed, given that the IBTrACS V_{max} data ($V_{max_{IB}}$) represent a combination of the environmental and TC wind fields. We optimize a series of the machine learning models were optimized by Randomized Search Cross-Validation with adopting mean square error RandomizedSearchCV tested as the loss function using Python v3.10.7. The models including a random forest (RF) algorithm, artificial neural network (ANN), convolutional neural network, support vector regressor, and multivariate linear regression (Table 2). In the above-mentioned models, we incorporate data for the entire period (1959–2022) were incorporated into the model training process. We randomly divide the dataset, made up of the input array and learning target, was randomly divided into two subsets, with 75% allocated for training and the remaining 25% for validation testing, following the methods of previous studies (e.g., Breiman, 2001; Guo et al., 2024). Training data for the entire period (1959–2022) were incorporated into the model training process. To optimize the model's performance, we opted for the MSE as the loss function. For a detailed account of the hyperparameter selections for each model, please refer to the Text S1 in supplementary materials. We found that RF provided the most robust predictions, as evidenced by higher Pearson correlation coefficients and smaller root mean square error (RMSE) values in most basins. To further assess the accuracy of the RF model, we define the error rate as the absolute relative errors between the predicted and observed V_{max} in the test data, normalized by the observations. The error rates are 0.13, 0.15, 0.22, 0.15, 0.19, 0.20, and 0.18, 0.22, 0.17 for the Western Pacific (WP), North Atlantic (NA), Eastern Pacific (EP), North Indian (NI), South Indian (SI) and South Pacific (SP) Western Pacific WP, North Atlantic, Eastern Pacific, North Indian, South Indian, and South Pacific and Eastern Pacific basins, respectively. NA Accordingly, we develop an RF regressor was developed to predict reconstructed V_{max} ($V_{max_{RC}}$), as follows:

$$V_{max_{RC}} = RF(V_0, V_{10}, V_{20}, \dots, V_{1000}, V_{TS}) \quad (1)$$

where RF and V_{TS} are the RF regressor and TC translation speed, respectively, and $V_0, V_{10}, V_{20}, \dots, V_{1000}$ refer to the 10 m azimuthal mean azimuthal wind speeds at radial distances from 0 to 1000 km. To further assess the accuracy of the RF model, we define the error rate of the random forest RF on the training data error rate as the absolute relative errors between the

222 ~~predicted and observed V_{max} in the test training data, normalized by the observations. The error rates are 0.131, 0.156,~~
 223 ~~0.22, 0.1509, 0.2019, and 0.186 and 0.220 for the Western Pacific (WP), North Atlantic (NA), Eastern Pacific (EP), North~~
 224 ~~Indian (NI), South Indian (SI), and South Pacific (SP) Eastern Pacific (EP) and basins, respectively.~~

225 ~~Table 2. Basic information on the comparison of the data derived from different model-derives with the observed V_{max}~~
 226 ~~data evaluation indices for V_{max} in Western Pacific (WP), North Atlantic (NA), Eastern Pacific (EP), North Indian (NI), South~~
 227 ~~Indian (SI) and South Pacific (SP) and Eastern Pacific (EP). CE, Pearson correlation coefficients; RMSE, root mean~~
 228 ~~square error. RF, random forecast; ANN, artificial neural network; CNN, convolutional neural network; SVR, support vector~~
 229 ~~regressor; MLR, multivariate linear regression.~~

	WP	NA	NI	SP	SI	EP
RF _{CE}	0.98	0.99	0.99	0.99	0.98	0.99
ANN _{CE}	0.98	0.99	0.99	0.98	0.99	0.97
CNN _{CE}	0.97	0.99	0.98	0.97	0.98	0.97
SVR _{CE}	0.99	0.99	0.98	0.99	0.99	0.99
MLR _{CE}	0.97	0.98	0.98	0.97	0.97	0.96
RF _{RMSE} (m/s)	2.60	4.09	1.33	3.73	3.25	5.05
ANN _{RMSE} (m/s)	5.09	5.31	1.65	3.87	4.37	10.05
CNN _{RMSE} (m/s)	5.92	8.39	2.43	7.18	7.30	11.2
SVR _{RMSE} (m/s)	3.99	6.70	2.18	4.87	5.03	9.08
MLR _{RMSE} (m/s)	7.33	9.34	2.28	7.42	7.45	12.49

230
 231 Similarly, ~~we use~~ variation in radial distance with azimuthal wind speed ~~was is used~~ to estimate R_{max} in the six basins.
 232 ~~After We also test testing ss~~ Several machine learning models ~~were are also tested~~ (Table 3). ~~Although the ANN-derived R_{max}~~
 233 ~~exhibited stronger correlations with observations, the root mean square error (RMSE) values of R_{max} derived by RF with~~
 234 ~~observations were are considerably smaller than that derived by other models. Therefore, we also utilize the RF regressor was~~
 235 ~~is utilized~~ to predict the reconstructed R_{max} (R_{max_RC}), as follows:

$$236 R_{max_RC} = RF(R_0, R_{0.01}, R_{0.02}, \dots, R_1) \quad (2)$$

237 where $R_0, R_{0.01}, R_{0.02}, \dots, R_1$ represent the radial distances at which normalized wind speeds range from 0 to 1, at an interval
 238 of 0.01. ~~In the RF models, the error rates are 0.1322+19, 0.15267+13, 0.228, 0.1564, 0.21094 and, 0.1875 and 0.28+3 for the~~
 239 ~~Western Pacific WP, North Atlantic A, Eastern Pacific P, North Indian I, South Indian I and, South Pacific P and EP basins,~~
 240 ~~respectively. We further evaluate~~ ~~The dataset, made up of the input array and learning target, was randomly divided into two~~
 241 ~~subsets, with 75% allocated for training and the remaining 25% for validation, following the methods of previous studies (e.g.,~~

Breiman, 2001; Guo et al., 2024). Training data for the entire period (1959–2022) were incorporated into the model training process. When optimizing the random forest model for regression tasks, we utilize Randomized Search Cross-Validation (RandomizedSearchCV) to systematically explore a wide range of hyperparameters. Specifically, we define hyperparameter distributions that encompass a range of values for the number of trees in the forest (100 to 300), maximum depth of the tree (10 to 30), maximum number of features (1 to 7), minimum number of samples (2 to 10), minimum number of samples (2 to 20), and maximum number of leaf nodes (800 to 1200). With 500 iterations and 5-fold cross-validation, we search for the optimal hyperparameter combination that minimizes the mean squared error, which is a common choice for regression problems due to its ability to penalize large errors. Leveraging parallel computing, we efficiently fit the model to the training data and obtain the best performing estimator. In the RF models, hyperparameters including the maximum tree depth, minimum leaf samples, minimum sample splits, and maximum leaf nodes were determined by randomized searches. The dataset, made up of the input array and learning target, was randomly divided into two subsets, with 75% allocated for training and the remaining 25% for validation, following the methods of previous studies (e.g., Breiman, 2001; Guo et al., 2024). Training data for the entire period (1959–2022) were incorporated into the model training process. Model performance was further evaluated by comparing the model-derived and observed V_{max} and R_{max} on the testing dataset in the Section 4 following sections, using a comprehensive set of statistical metrics, including mean error, mean absolute error (MAE), root mean square error (RMSE), and Pearson correlation coefficients. The statistical significance of Pearson correlation coefficients is evaluated through the application of a t-test.

Table 3. Similar to Table 2, but for R_{max} .

	<u>WP</u>	<u>NA</u>	<u>NI</u>	<u>SP</u>	<u>SI</u>	<u>EP</u>
<u>RF_{CE}</u>	<u>0.93</u>	<u>0.96</u>	<u>0.96</u>	<u>0.91</u>	<u>0.96</u>	<u>0.93</u>
<u>ANN_{CE}</u>	<u>0.96</u>	<u>0.97</u>	<u>0.93</u>	<u>0.97</u>	<u>0.96</u>	<u>0.94</u>
<u>CNN_{CE}</u>	<u>0.95</u>	<u>0.96</u>	<u>0.95</u>	<u>0.97</u>	<u>0.94</u>	<u>0.96</u>
<u>SVR_{CE}</u>	<u>0.06</u>	<u>0.21</u>	<u>0.26</u>	<u>0.25</u>	<u>0.01</u>	<u>0.07</u>
<u>MLR_{CE}</u>	<u>0.90</u>	<u>0.93</u>	<u>0.98</u>	<u>0.98</u>	<u>0.96</u>	<u>0.84</u>
<u>RF_{RMSE} (km)</u>	<u>20.80</u>	<u>31.47</u>	<u>10.48</u>	<u>15.11</u>	<u>16.51</u>	<u>24.75</u>
<u>ANN_{RMSE} (km)</u>	<u>31.96</u>	<u>46.74</u>	<u>16.62</u>	<u>21.06</u>	<u>23.22</u>	<u>41.14</u>
<u>CNN_{RMSE} (km)</u>	<u>34.93</u>	<u>52.89</u>	<u>22.04</u>	<u>20.97</u>	<u>25.69</u>	<u>44.07</u>
<u>SVR_{RMSE} (km)</u>	<u>43.53</u>	<u>72.43</u>	<u>28.26</u>	<u>29.05</u>	<u>30.99</u>	<u>51.15</u>

260

261 **3.3 Empirical wind speed–pressure relationship for determining P_{min}**

262 ~~We model t~~The conversion between V_{max} and P_{min} at a given time point during a TC ~~was is modeled~~ using the empirical
263 wind–pressure relationship (Atkinson and Holliday, 1977; Harper, 2002), as follows:

$$264 V_{max} = a(P_{env} - P_{min})^b \quad (3)$$

265 where P_{env} is the environmental pressure obtained from the mean SLP for the TC center location 1–10 days earlier based on
266 the ERA5 data, following the method of Bloemendaal et al. (2020); ~~we estimate~~ a and b ~~are were estimated~~ in each basin
267 using a nonlinear least squares approach, based on V_{max} and the corresponding P_{min} of the IBTrACS dataset. V_{max_RC} ~~was~~
268 ~~is~~ input into the fitted Eq. (3) to obtain the reconstructed P_{min} (P_{min_RC}).

269

270

271 **3.4 TC radial wind profile models for computing R_{34} , R_{50} , and R_{64}**

272 Previous studies have developed TC radial wind profile models for estimating TC structures (e.g., Pérez-Alarcón et al., 2021).

273 After obtaining the reconstructed V_{max} and R_{max} , [we utilize](#) six widely used wind field models (Holland, 1980; DeMaria,274 1987; Willoughby et al., 2006; Emanuel and Rotunno, 2011; Frisius and Scgönemann, 2013; Chavas et al., 2015), ~~were are~~275 ~~used~~ to estimate the reconstructed TC R_{34} , R_{50} , and R_{64} (R_{34_RC} , R_{50_RC} , and R_{64_RC}). [For a detailed description of the wind](#)276 [profile modelshyperparameter selections for each model, please refer to the Text S12 in supplementary materials.](#)277 [We evaluate the performance of each profile model by comparing \$R_{34}\$, \$R_{50}\$, and \$R_{64}\$ estimates with those](#)278 [recorded in the IBTrACS dataset. Subsequently, wWe selectselect theThe optimal model—is selected to generate](#)279 [reconstructed \$R_{34}\$, \$R_{50}\$, and \$R_{64}\$, as described in detail in Section 4.](#)

280

281

282 The wind profile model proposed by Holland (1980) was formulated as follows:

283
$$V(r) = V_{max} \sqrt{\left(\frac{R_{max}}{r}\right)^b e^{1 - \left(\frac{r}{R_{max}}\right)^{-b}}} \quad (4)$$

284 where V is the wind speed at distance r from the TC center, and $b = 2$, according to Kowaleski and Evans (2016).

285 The model developed by DeMaria (1987) was formulated as follows:

286
$$V(r) = V_{max} \left(\frac{R_{max}}{r}\right)^{\frac{1}{e}} e^{\frac{1 - \left(\frac{r}{R_{max}}\right)^e}{d}} \quad (5)$$

287 where $e = 0.63$ and $d = 1$, following Kowaleski and Evans (2016).

288 The model proposed by Willoughby et al. (2006; hereinafter, W06) was formulated as follows:

289
$$V(r) = \begin{cases} V_{max} \left(\frac{r}{R_{max}}\right)^{\beta}, & 0 \leq r \leq R_1 \\ V_1(1-w) + V_0 w, & R_1 \leq r \leq R_2 \\ V_{max} e^{\frac{r - R_{max}}{\alpha}}, & R_2 \leq r \end{cases} \quad (6)$$

where V_i and V_o are the tangential wind components in the eye and beyond the transition zone, respectively, and w , X_i , and n are the weight function, exponential decay length in the outer vortex, and power law exponent within the eye, respectively.

The model proposed by Emanuel and Rotunno (2011) was formulated as follows:

$$V(r) = \frac{2r(R_{max}V_{max} + 0.5fR_{max}^2)}{R_{max}^2 + r^2} - \frac{fr}{2} \quad (7)$$

where f is the Coriolis parameter.

The model developed by Frisius and Segönemann (2013) was formulated as follows:

$$V(r) = V_{max} \frac{r}{R_{max}} \left[\frac{2\left(\frac{R_{max}}{r}\right)^2}{2 - \left(\frac{C_H}{C_D}\right)\left[1 - \left(\frac{r}{R_{max}}\right)^2\right]} \right]^{\frac{1}{2}} \frac{C_H}{C_D} - \frac{fr}{2} \quad (8)$$

where C_H and C_D are the surface enthalpy transfer and drag coefficients, respectively, and $\frac{C_H}{C_D} = 1$, according to Frisius and Segönemann (2013).

The model proposed by Chavas et al. (2015; hereinafter, CLE15) was formulated as follows:

$$\left(\frac{M_{inner}}{M_m}\right)^2 \frac{C_k}{C_a} = \frac{2\left(\frac{r}{R_{max}}\right)^2}{2 - \left(\frac{C_k}{C_a}\right) + \left(\frac{C_k}{C_a}\right)\left(\frac{r}{R_{max}}\right)^2} \quad (9)$$

$$\frac{\partial M_{outer}}{\partial r} = \frac{C_a(rV)^2}{0.001(r_o^2 - r^2)}$$

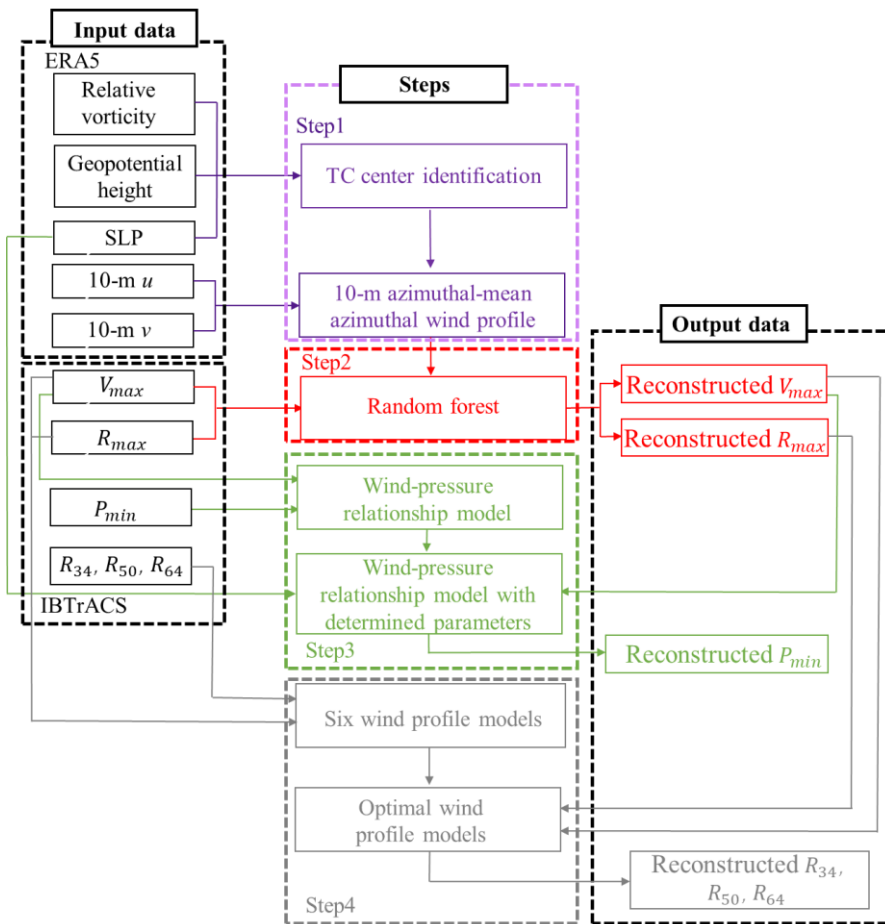
where M_{inner} , M_{outer} , and M_m are the angular moment of the inner and outer wind regimes and at R_{max} , respectively; and C_k and C_a are the exchange surface enthalpy and momentum coefficients, respectively.

The performance of each profile model was is evaluated by comparing R_{34} , R_{50} , and R_{64} estimates with those recorded in the IBTrACS dataset. The optimal model was is selected to generate reconstructed R_{34} , R_{50} , and R_{64} , as described in detail in Section 4.

3.5 Flowchart for optimal wind profile model selection

After identifying the TC center, we use an RF approach to estimate V_{max} and R_{max} based on the ERA5-derived TC 10 m azimuthal mean azimuthal wind profiles. We evaluate model performance by comparing the model-derived and observed V_{max} and R_{max} on the testing dataset, using a comprehensive set of statistical metrics. Next, we estimate the parameters of

312 the empirical wind–pressure relationship ~~were are estimated~~, and ~~compute~~ TC P_{min} values ~~were are computed~~. Finally, ~~we~~
 313 ~~derive~~ the TC R_{34} , R_{50} , and R_{64} ~~were are derived~~ by selecting the optimal wind profile model from among the six widely
 314 used models. The overall methodology is illustrated in Fig. 3.–

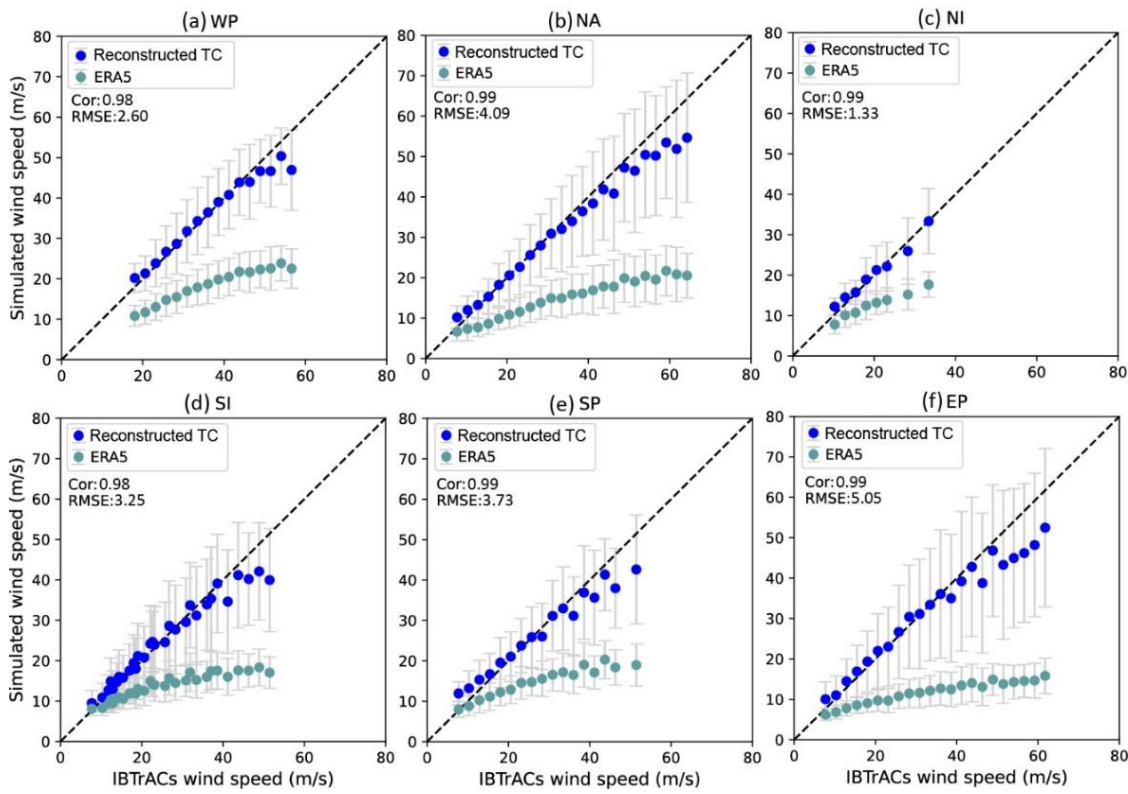


315
 316 **Figure 3: Flowchart with the tropical cyclone center identification and wind profiles extracted from ERA5 (Step 1; in purple), the**
 317 **10-m maximum wind speeds and radii to maximum winds estimated by random forest model (Step 2; in red), the minimum central**
 318 **pressure estimated by empirical wind-pressure relationship (Step 3; in green), and the out size estimated by wind profile models**
 319 **(Step 4; in grey).**

320 **4. Results and Discussion**

321 ~~We evaluate t~~The accuracy of the V_{max_RC} model results ~~was is evaluated~~ according to various statistical metrics based on
 322 the testing datasets (Fig. 4), as prescribed by Breiman (2001). The V_{max_RC} data ~~were are~~ strongly correlated with
 323 observations, with correlation coefficients exceeding 0.98 for all six basins. The RMSE values for the ~~WP, NA, NI, SI, SP and~~
 324 ~~EP~~West Pacific, North Atlantic, North and South Indian Ocean, and South and East Pacific basins ~~were are~~ 2.60, 4.09, 1.33,
 325 3.25, 3.73, and 5.05 m/s, respectively. Compared to V_{max_ERA5} , the reconstruction ~~provideprovides~~ a reduction in the ~~mean~~
 326 ~~absolute bias~~MAE of over 10 m/s in most basins, with a further reduction of 19.62 m/s in the East Pacific basin, as described

327 in detail in Table 24. The model was is more effective at reducing biases between ERA5-derived results and observations for
 328 larger V_{max} values. Furthermore, given the high influence of ENSO on TC intensity (Chu, 2024), we also evaluate the
 329 accuracy of V_{max_RC} was is evaluated for moderate to strong El Niño and La Niña years (Fig. S2 and S3). We also observed
 330 a high degree of correlation coefficients (>0.97) and low RMSE values ($<5\text{m/s}$) were are observed between V_{max_RC} and
 331 V_{max} in all six basins during ENSO years. These metrics clearly demonstrate the superior better accuracy of V_{max_RC} and its
 332 reduced bias compared to V_{max_ERA5} .

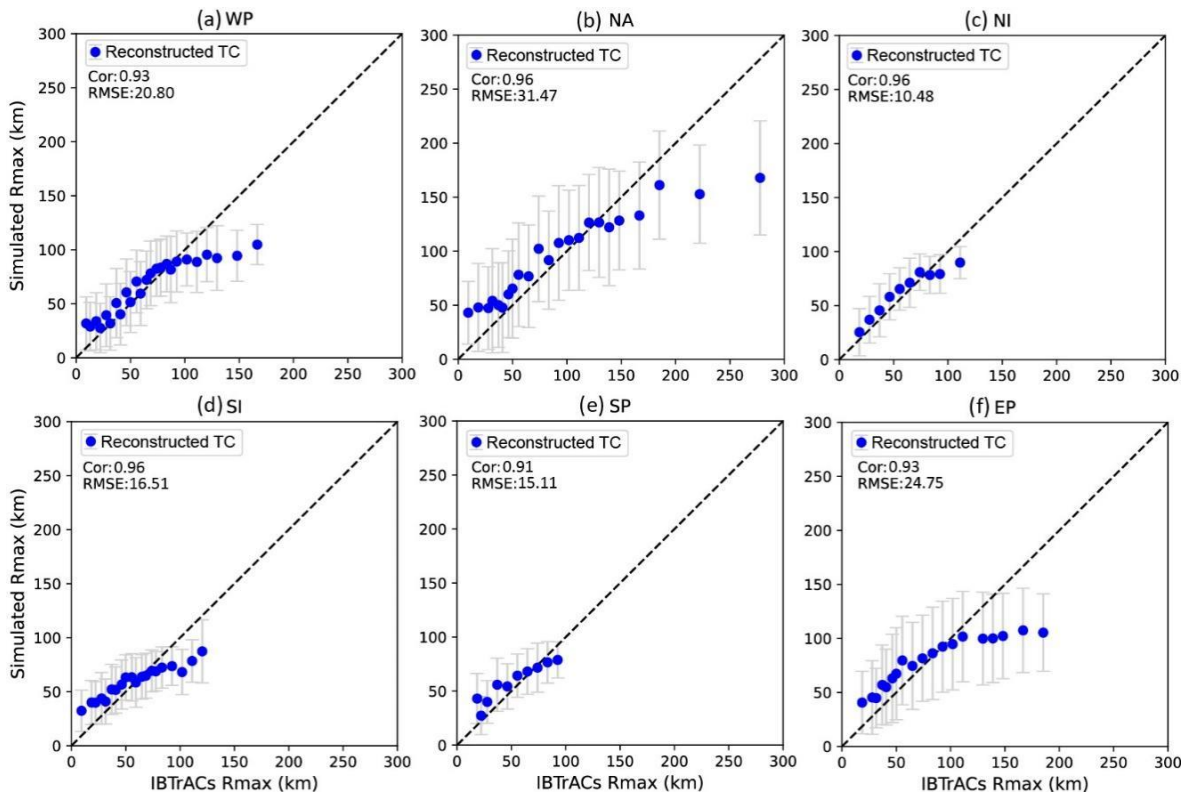


333
 334 **Figure 4:** Comparison between value-averaged maximum wind speeds (V_{max}) from ERA5-derived and reconstructed (ERA5 +
 335 Random forest) data and IBTrACS maximum wind speeds for tropical cyclones in (a) Western Pacific, (b) North Atlantic, (c) North
 336 Indian, (d) South Indian, (e) South Pacific and (f) Eastern Pacific basins. Grey lines represent the error bar, given as one standard
 337 deviation from the mean. The values with sample sizes less than 30 in IBTrACS were are excluded.
 338

Table 24: Basic information on [the comparison of the ERA-5-derived and reconstructed data with the observation data](#) evaluation indices for V_{max} . ME, mean errors; MAE, mean-of-the absolute biaserror; RMSE, root mean square error; CE, correlation coefficients.

	ME (m/s)	MAE (m/s)	RMSE (m/s)	CE
Global _{ERA5}	16.73	16.80	21.70	0.92
Global _{Reconstructed}	2.82	2.83	4.34	0.99
WP _{ERA5}	18.93	18.93	20.54	0.97
WP _{Reconstructed}	0.56	1.63	2.60	0.98
NA _{ERA5}	21.03	21.03	24.46	0.98
NA _{Reconstructed}	2.38	2.82	4.09	0.99
NI _{ERA5}	7.74	7.74	8.96	0.98
NI _{Reconstructed}	-0.25	1.11	1.33	0.99
SI _{ERA5}	12.39	12.41	15.61	0.93
SI _{Reconstructed}	0.71	2.17	3.25	0.98
SP _{ERA5}	13.71	13.73	16.67	0.96
SP _{Reconstructed}	1.19	2.70	3.73	0.99
EP _{ERA5}	23.09	23.09	26.86	0.97
EP _{Reconstructed}	2.36	3.47	5.05	0.99

We similarly evaluated the accuracy of R_{max_RC} for the six basins based on the testing datasets (Fig. 5). Correlation coefficients between R_{max_RC} and R_{max} recorded in IBTrACS (R_{max_IB}) exceeded 0.9, indicating strong correlation between the reconstructed results and observations. Moreover, the RMSEs for the [West Pacific WP](#), [North Atlantic A](#), [North NI](#) and [South Indian Ocean SI](#), and [South SP](#) and [East Pacific P](#) basins were 20.80, 31.47, 10.48, 16.51, 15.11, and 24.75 km, respectively. Importantly, R_{max_ERA5} exhibited a large deviation from observations, exceeding 300 km at very low R_{max_IB} values. Therefore, for clarity, the R_{max_ERA5} data are not shown with the reconstructed TC results in Fig. 5. The [mean of the absolute bias error \(MAEW\)](#) exhibited a reduction of 39.57 km on a global scale, with a further reduction of over 59.37 km in the [South Indian Ocean SI](#) basin, as described in detail in Table 35. [It is noteworthy that the error bars are larger for the North Atlantic A and East Pacific P basins in comparison to the other basins. This may be attributed to the low correlations between \$R_{max}\$ in IBTrACS and in ERA5 \(NA: 0.37; EP: -0.02\).](#) Although the R_{max_RC} data slightly overestimated observations at low R_{max_IB} values and underestimated observations at high R_{max_IB} values, they greatly reduced biases compared to the R_{max_ERA5} data, and thus produced [superior better](#) predictions for all six basins.



354
 355
 356

Figure 5. Similar to Figure 4, but for radii to maximum winds (R_{max}).

357

358

Table 35: Similar to Table 24, but for R_{max} .

	ME (km)	MAE (km)	RMSE (km)	CE
Global _{ERA5}	-41.64	<u>55.49</u> 15.92	67.66	0.44
Global _{Reconstructed}	1.37	<u>55.49</u> 15.92	22.19	0.94
WP _{ERA5}	-56.43	58.31	69.86	0.75
WP _{Reconstructed}	1.32	14.93	20.80	0.93
NA _{ERA5}	-7.79	54.25	64.59	0.37
NA _{Reconstructed}	4.05	21.44	31.47	0.96
NI _{ERA5}	-28.95	29.39	33.75	0.96
NI _{Reconstructed}	-2.30	9.65	10.48	0.96
SI _{ERA5}	-73.40	73.48	88.39	0.74
SI _{Reconstructed}	-1.50	14.11	16.51	0.96
SP _{ERA5}	-52.42	52.99	61.95	0.90
SP _{Reconstructed}	-3.21	12.09	15.11	0.91
EP _{ERA5}	-24.31	47.83	56.59	-0.02
EP _{Reconstructed}	6.91	18.83	24.75	0.93

359

[We compute](#)

360

361 P_{min_RC} ~~was is computed~~ based on an empirical wind–pressure relationship. We employ V_{max_IB} and the corresponding

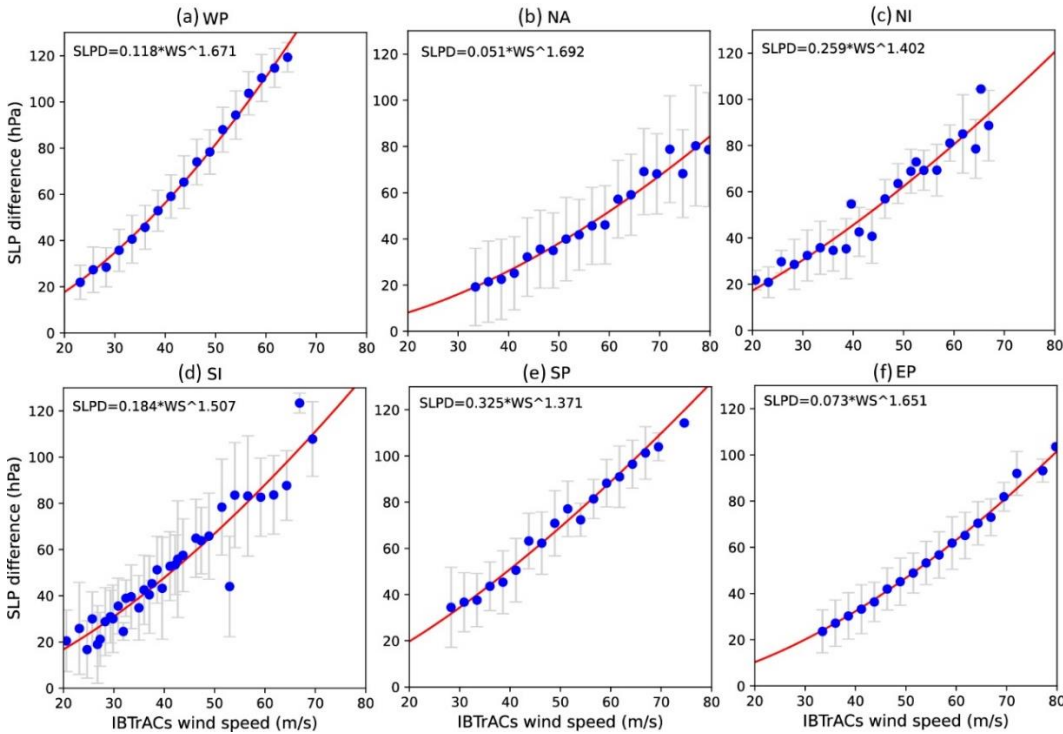
362 P_{min} recorded in IBTrACS (P_{min_IB}) ~~were are also employed~~ in the reconstruction, and we obtain P_{env} ~~was is obtained~~ from

363 the ERA5 dataset, following the method of Bloemendaal et al. (2020). We estimate r Related parameters ~~were are estimated~~

364 through nonlinear fitting; the results are shown in Fig. 6. For the WP, NA, NI, SI, SP and EP ~~West Pacific, North Atlantic,~~

365 North and South Indian Ocean, and South and East Pacific basins, we used a values of 0.118, 0.051, 0.259, 0.184, 0.325, and

366 0.073 and b values of 1.67, 1.692, 1.402, 1.507, 1.371, and 1.651, respectively, in Eq. (3).



367 **Figure 6: Similar to Figure 4, but for non-linear regression analyses between value-averaged IBTrACS maximum wind**
368 **speeds and sea level pressurethe difference between environmental pressure and typical cyclone minimum central**
369 **pressure (SLPD).**
370

371 The mean and standard deviation values of various TC characteristics based on the testing datasets are plotted in Fig. 7

372 to compare the overall performance of the model in reconstructing TCs. Mean biases in R_{max} and P_{min} between the

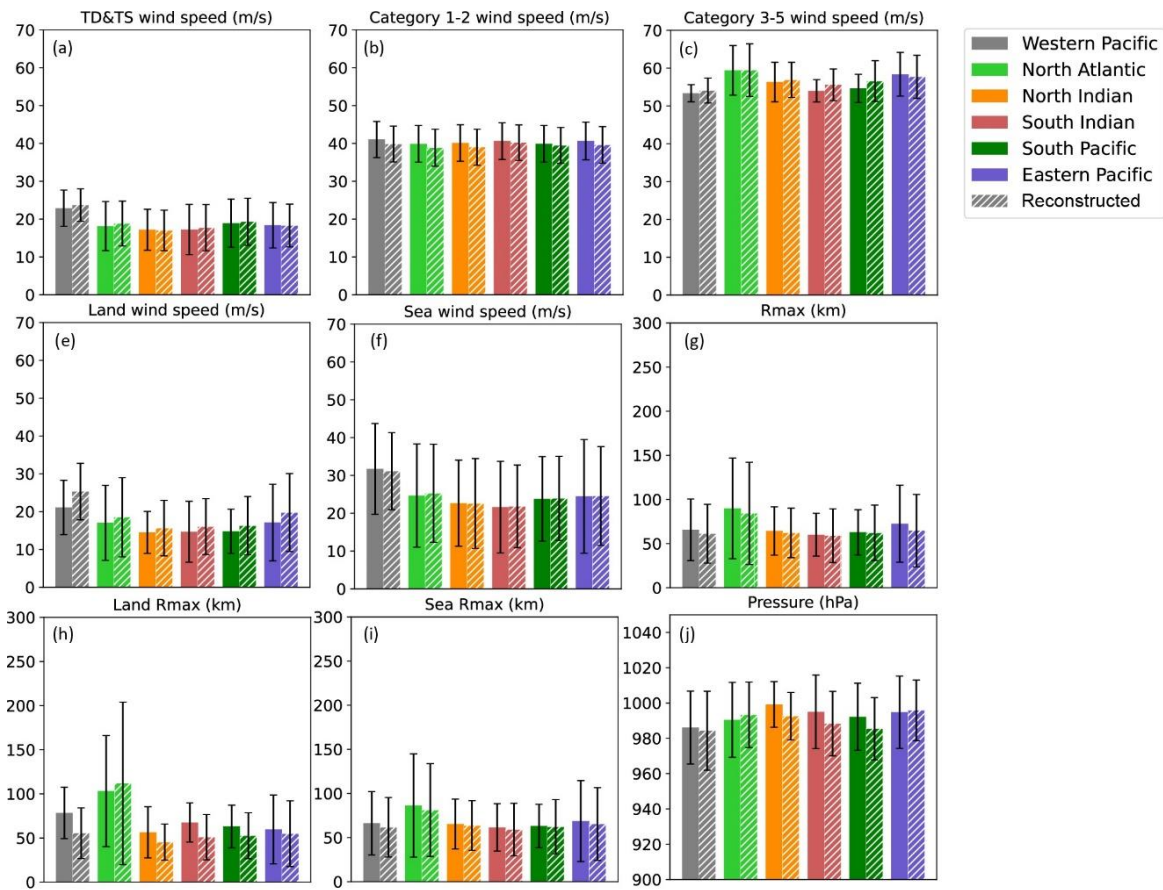
373 reconstructed TC and IBTrACS datasets ~~were are~~ both <3% in most basins, providing compelling evidence that the predictions

374 ~~were are~~ in good agreement with observations. In contrast to those over the sea, the reconstructed dataset overestimate and

375 underestimate landfall TC V_{max} and R_{max} ~~data were are overestimated and underestimated~~ in most basins, respectively,

376 likely due to the decay of TC wind speeds after landfall, which is not considered in the RF-based models. Despite these

377 differences, biases remained within 5% in most basins, indicating that the reconstructed landfall TC characteristics were are
 378 closely aligned with those in the IBTrACS dataset.



379
 380 **Figure 7: Bar charts for comparing the mean value of the different tropical cyclone characteristics. Each of the colors indicates a**
 381 **different basin. Solid and dashed bars represent IBTrACS and reconstructed tropical cyclone data, respectively.**

382 After obtaining the reconstructed TC intensity dataset, we use six widely used models were are used to estimate R_{34_RC} ,
 383 R_{50_RC} , and R_{64_RC} . We conducted a comparative analysis of the model-derived results and observations to determine which
 384 radial wind profile estimate more closely approximated the TC outer radius, based on various statistical metrics (Table S46S1–
 385 S61+S6). In the WP basin, the W06 model demonstrates the strongest correlation in WP basin. The the W06 model results
 386 exhibited strongest correlation, (R_{34} : 0.89, R_{50} : 0.82, R_{64} : 0.78), achieving the lowest RMSE and mean absolute error
 387 (MAE) lowest RMSE (R_{34} : 0.89, R_{50} : 0.82, R_{64} : 0.78), and lowest absolute mean absolute error (MAE). In NA basin, the
 388 CLE15 model outperforms others for the CLE15 model performs better for R_{34} , with a correlation coefficient of 0.87, RMSE
 389 of 78.77 km, and MAE of 53 km, whereas the W06 model performs better for with the correlation coefficient of 0.87, RMSE
 390 of 78.77 km and MAE of 53 km, whereas the W06 model results show a better performance for R_{50} and R_{64} . For the NI and

391 SI basins, all models except W06 show poor correlation with observations, some even exhibiting negative correlations. In the
392 SP and EP basins, W06 substantially significantly surpasses other models in terms of correlation coefficient. Although other
393 models produce slightly smaller RMSE and MAE values for In NI and SI basins, with the exception of W06, the results of the
394 remaining models exhibit a poor correlation with observations, with some even demonstrating a negative correlation.the W06
395 model results exhibit strongest correlation. In SP and EP basins, W06 remains the substantially higher correlation
396 coefficient than other models,for all basins except the North AtlanticNA basin, whereas the CLE15 model performed better
397 for R_{34_RC} in the NA basinNorth Atlantic basin. While the RMSE and MAE of R_{64} in the EP basin compared to W06, their
398 correlation coefficients, which are below < 0.2, justify our choice of W06. Consequently, we select W06 to forecast derived by
399 other models are marginally smaller those simulated by W06 in EP basin, their correlation coefficients of less than 0.2 lead
400 use to select W06. Therefore, we used W06 to forecast R_{34_RC} , R_{50_RC} , and R_{64_RC} for the West PacificWP, North and South
401 Indian OceanNI, SI, SP, and South and EPast Pacific basins, whereas for the North AtlanticNA basin, we used CLE15 to
402 predict R_{34_RC} and W06 to predict R_{50_RC} and R_{64_RC} . The correlation coefficients were are >0.75 for three outer size
403 metrics in most basins (Table 4S16).

404 Table S16. Basic information on the comparison of the reconstructed data with the observational data for R_{34} , R_{50} and R_{64} . ME,
405 mean errors; MAE, mean of the absolute biaserror; RMSE, root mean square error; CE, correlation coefficients. H80, D87, W06,
406 E11, F13 and CLE15 refer to the wind field models proposed by Holland (1980), DeMaria (1987), Willoughby et al. (2006), Emanuel
407 and Rotunno (2011), Frisius and Scgönemann (2013) and Chavas et al. (2015)

	Optimal profile	ME (km)	MAE (km)	RMSE (km)	CE
WP _{R34}	W06	-24.79	46.75	64.54	0.89
WP _{R50}	W06	-14.60	26.00	33.27	0.82
WP _{R64}	W06	-14.14	18.28	22.71	0.78
NA _{R34}	CLE15	-25.19	53.00	78.77	0.87
NA _{R50}	W06	-11.58	32.71	57.39	0.84
NA _{R64}	W06	2.67	18.52	30.37	0.87
NI _{R34}	W06	-23.19	31.19	41.59	0.74
NI _{R50}	W06	-14.66	20.49	25.69	0.63
NI _{R64}	W06	-11.63	16.62	21.17	0.62
SI _{R34}	W06	3.57	45.71	56.68	0.74
SI _{R50}	W06	14.35	29.69	36.18	0.46
SI _{R64}	W06	9.68	18.54	21.57	0.43
SP _{R34}	W06	-5.00	33.51	46.25	0.83

<u>SP_{R50}</u>	<u>W06</u>	<u>11.75</u>	<u>21.53</u>	<u>27.25</u>	<u>0.77</u>
<u>SP_{R64}</u>	<u>W06</u>	<u>12.75</u>	<u>15.60</u>	<u>18.56</u>	<u>0.77</u>
<u>EP_{R34}</u>	<u>W06</u>	<u>32.25</u>	<u>44.43</u>	<u>51.31</u>	<u>0.81</u>
<u>EP_{R50}</u>	<u>W06</u>	<u>27.19</u>	<u>31.77</u>	<u>36.61</u>	<u>0.68</u>
<u>EP_{R64}</u>	<u>W06</u>	<u>18.74</u>	<u>21.66</u>	<u>25.24</u>	<u>0.51</u>

408

409

Table 7. Similar to Table S16, but in North Atlantic.

	<u>ME (km)</u>	<u>MAE (km)</u>	<u>RMSE (km)</u>	<u>CE</u>
<u>H80_{R34}</u>	<u>50.20</u>	<u>63.41</u>	<u>89.89</u>	<u>0.87</u>
<u>D87_{R34}</u>	<u>22.85</u>	<u>58.87</u>	<u>82.83</u>	<u>0.85</u>
<u>W06_{R34}</u>	<u>41.75</u>	<u>67.06</u>	<u>112.55</u>	<u>0.81</u>
<u>E11_{R34}</u>	<u>19.90</u>	<u>54.17</u>	<u>80.59</u>	<u>0.85</u>
<u>F13_{R34}</u>	<u>91.60</u>	<u>94.33</u>	<u>122.41</u>	<u>0.87</u>
<u>CLE15_{R34}</u>	<u>25.19</u>	<u>53.00</u>	<u>78.77</u>	<u>0.87</u>
<u>H80_{R50}</u>	<u>25.33</u>	<u>43.75</u>	<u>62.34</u>	<u>0.82</u>
<u>D87_{R50}</u>	<u>6.81</u>	<u>45.40</u>	<u>66.86</u>	<u>0.79</u>
<u>W06_{R50}</u>	<u>11.58</u>	<u>32.71</u>	<u>57.39</u>	<u>0.84</u>
<u>E11_{R50}</u>	<u>25.41</u>	<u>61.73</u>	<u>89.89</u>	<u>0.82</u>
<u>F13_{R50}</u>	<u>50.70</u>	<u>54.88</u>	<u>72.66</u>	<u>0.83</u>
<u>CLE15_{R50}</u>	<u>10.75</u>	<u>41.50</u>	<u>60.52</u>	<u>0.82</u>
<u>H80_{R64}</u>	<u>15.35</u>	<u>27.55</u>	<u>39.46</u>	<u>0.82</u>
<u>D87_{R64}</u>	<u>6.39</u>	<u>26.98</u>	<u>39.04</u>	<u>0.81</u>
<u>W06_{R64}</u>	<u>2.67</u>	<u>18.52</u>	<u>30.37</u>	<u>0.87</u>
<u>E11_{R64}</u>	<u>8.73</u>	<u>26.15</u>	<u>37.58</u>	<u>0.83</u>
<u>F13_{R64}</u>	<u>27.81</u>	<u>31.47</u>	<u>42.17</u>	<u>0.85</u>
<u>CLE15_{R64}</u>	<u>5.52</u>	<u>26.38</u>	<u>37.92</u>	<u>0.83</u>

Table 8. Similar to Table S16, but in North Indian.

	<u>ME (km)</u>	<u>MAE (km)</u>	<u>RMSE (km)</u>	<u>CE</u>
<u>H80_{R34}</u>	<u>71.01</u>	<u>72.12</u>	<u>87.65</u>	<u>0.17</u>
<u>D87_{R34}</u>	<u>62.28</u>	<u>64.64</u>	<u>81.20</u>	<u>0.18</u>
<u>W06_{R34}</u>	<u>23.19</u>	<u>31.19</u>	<u>41.59</u>	<u>0.74</u>
<u>E11_{R34}</u>	<u>59.22</u>	<u>61.89</u>	<u>77.41</u>	<u>0.27</u>
<u>F13_{R34}</u>	<u>88.25</u>	<u>88.42</u>	<u>102.12</u>	<u>0.12</u>
<u>CLE15_{R34}</u>	<u>59.04</u>	<u>61.77</u>	<u>78.04</u>	<u>0.22</u>
<u>H80_{R50}</u>	<u>40.23</u>	<u>41.11</u>	<u>49.98</u>	<u>-0.17</u>
<u>D87_{R50}</u>	<u>32.57</u>	<u>35.01</u>	<u>45.31</u>	<u>-0.24</u>
<u>W06_{R50}</u>	<u>14.66</u>	<u>20.49</u>	<u>25.69</u>	<u>0.63</u>
<u>E11_{R50}</u>	<u>20.03</u>	<u>37.42</u>	<u>43.99</u>	<u>-0.57</u>
<u>F13_{R50}</u>	<u>49.46</u>	<u>50.07</u>	<u>57.74</u>	<u>-0.29</u>
<u>CLE15_{R50}</u>	<u>32.77</u>	<u>34.95</u>	<u>44.63</u>	<u>-0.18</u>
<u>H80_{R64}</u>	<u>24.54</u>	<u>27.28</u>	<u>33.41</u>	<u>-0.18</u>
<u>D87_{R64}</u>	<u>19.30</u>	<u>24.63</u>	<u>30.47</u>	<u>-0.23</u>
<u>W06_{R64}</u>	<u>11.63</u>	<u>16.62</u>	<u>21.17</u>	<u>0.62</u>
<u>E11_{R64}</u>	<u>22.20</u>	<u>25.82</u>	<u>31.92</u>	<u>-0.19</u>
<u>F13_{R64}</u>	<u>29.87</u>	<u>31.81</u>	<u>38.26</u>	<u>-0.47</u>
<u>CLE15_{R64}</u>	<u>18.94</u>	<u>24.54</u>	<u>30.71</u>	<u>-0.33</u>

421

Table 9. Similar to Table S16, but in South Indian.

	<u>ME (km)</u>	<u>MAE (km)</u>	<u>RMSE (km)</u>	<u>CE</u>
<u>H80_{R34}</u>	<u>52.37</u>	<u>66.93</u>	<u>86.54</u>	<u>0.40</u>
<u>D87_{R34}</u>	<u>39.35</u>	<u>65.36</u>	<u>83.62</u>	<u>0.24</u>
<u>W06_{R34}</u>	<u>3.57</u>	<u>45.71</u>	<u>56.68</u>	<u>0.74</u>
<u>E11_{R34}</u>	<u>32.10</u>	<u>58.83</u>	<u>75.18</u>	<u>0.42</u>
<u>F13_{R34}</u>	<u>77.33</u>	<u>82.86</u>	<u>103.96</u>	<u>0.40</u>
<u>CLE15_{R34}</u>	<u>34.01</u>	<u>58.82</u>	<u>75.05</u>	<u>0.46</u>
<u>H80_{R50}</u>	<u>16.33</u>	<u>33.34</u>	<u>42.84</u>	<u>0.06</u>
<u>D87_{R50}</u>	<u>4.94</u>	<u>33.45</u>	<u>41.81</u>	<u>-0.01</u>
<u>W06_{R50}</u>	<u>14.35</u>	<u>29.69</u>	<u>36.18</u>	<u>0.46</u>
<u>E11_{R50}</u>	<u>10.50</u>	<u>40.17</u>	<u>49.96</u>	<u>-0.13</u>
<u>F13_{R50}</u>	<u>31.74</u>	<u>39.51</u>	<u>50.65</u>	<u>-0.01</u>
<u>CLE15_{R50}</u>	<u>6.01</u>	<u>33.58</u>	<u>41.64</u>	<u>0.02</u>
<u>H80_{R64}</u>	<u>6.23</u>	<u>18.45</u>	<u>23.88</u>	<u>-0.01</u>
<u>D87_{R64}</u>	<u>2.01</u>	<u>18.92</u>	<u>23.27</u>	<u>0.05</u>
<u>W06_{R64}</u>	<u>9.68</u>	<u>18.54</u>	<u>21.57</u>	<u>0.43</u>
<u>E11_{R64}</u>	<u>-0.55</u>	<u>18.31</u>	<u>22.70</u>	<u>0.12</u>
<u>F13_{R64}</u>	<u>17.11</u>	<u>21.82</u>	<u>28.37</u>	<u>-0.06</u>
<u>CLE15_{R64}</u>	<u>0.36</u>	<u>18.21</u>	<u>22.42</u>	<u>0.13</u>

422

423

Table 10. Similar to Table S16, but in South Pacific.

	<u>ME (km)</u>	<u>MAE (km)</u>	<u>RMSE (km)</u>	<u>CE</u>
<u>H80_{R34}</u>	<u>59.42</u>	<u>67.85</u>	<u>82.65</u>	<u>0.66</u>
<u>D87_{R34}</u>	<u>46.49</u>	<u>61.37</u>	<u>77.34</u>	<u>0.57</u>
<u>W06_{R34}</u>	<u>5.00</u>	<u>33.51</u>	<u>46.25</u>	<u>0.83</u>
<u>E11_{R34}</u>	<u>39.66</u>	<u>53.81</u>	<u>67.68</u>	<u>0.69</u>
<u>F13_{R34}</u>	<u>85.65</u>	<u>88.49</u>	<u>104.22</u>	<u>0.68</u>
<u>CLE15_{R34}</u>	<u>40.36</u>	<u>53.51</u>	<u>67.32</u>	<u>0.71</u>
<u>H80_{R50}</u>	<u>21.77</u>	<u>30.51</u>	<u>36.71</u>	<u>0.64</u>
<u>D87_{R50}</u>	<u>11.07</u>	<u>26.03</u>	<u>32.12</u>	<u>0.63</u>
<u>W06_{R50}</u>	<u>11.75</u>	<u>21.53</u>	<u>27.25</u>	<u>0.77</u>
<u>E11_{R50}</u>	<u>2.86</u>	<u>29.22</u>	<u>38.00</u>	<u>0.42</u>
<u>F13_{R50}</u>	<u>38.11</u>	<u>41.99</u>	<u>49.05</u>	<u>0.62</u>
<u>CLE15_{R50}</u>	<u>10.19</u>	<u>24.78</u>	<u>31.18</u>	<u>0.65</u>
<u>H80_{R64}</u>	<u>2.51</u>	<u>13.33</u>	<u>16.38</u>	<u>0.64</u>
<u>D87_{R64}</u>	<u>5.80</u>	<u>14.17</u>	<u>17.05</u>	<u>0.66</u>
<u>W06_{R64}</u>	<u>12.75</u>	<u>15.60</u>	<u>18.56</u>	<u>0.77</u>
<u>E11_{R64}</u>	<u>4.97</u>	<u>14.14</u>	<u>17.02</u>	<u>0.68</u>
<u>F13_{R64}</u>	<u>13.60</u>	<u>16.42</u>	<u>20.91</u>	<u>0.66</u>

~~CLE15_{R64} 7.00 14.58 17.05 0.69~~

424

425

Table 11. Similar to Table S16, but in Eastern Pacific.

	<u>ME (km)</u>	<u>MAE (km)</u>	<u>RMSE (km)</u>	<u>CE</u>
<u>H80_{R34}</u>	<u>-18.13</u>	<u>48.97</u>	<u>62.66</u>	<u>0.52</u>
<u>D87_{R34}</u>	<u>-7.32</u>	<u>55.07</u>	<u>69.07</u>	<u>0.41</u>
<u>W06_{R34}</u>	<u>32.25</u>	<u>44.43</u>	<u>51.31</u>	<u>0.81</u>
<u>E11_{R34}</u>	<u>4.02</u>	<u>50.50</u>	<u>64.00</u>	<u>0.53</u>
<u>F13_{R34}</u>	<u>-43.59</u>	<u>55.90</u>	<u>70.91</u>	<u>0.54</u>
<u>CLE15_{R34}</u>	<u>5.97</u>	<u>48.36</u>	<u>61.56</u>	<u>0.57</u>
<u>H80_{R50}</u>	<u>-9.60</u>	<u>27.55</u>	<u>36.73</u>	<u>0.32</u>
<u>D87_{R50}</u>	<u>-2.51</u>	<u>28.81</u>	<u>38.34</u>	<u>0.27</u>
<u>W06_{R50}</u>	<u>27.19</u>	<u>31.77</u>	<u>36.61</u>	<u>0.68</u>
<u>E11_{R50}</u>	<u>10.68</u>	<u>35.00</u>	<u>47.12</u>	<u>0.12</u>
<u>F13_{R50}</u>	<u>-23.54</u>	<u>31.68</u>	<u>40.92</u>	<u>0.31</u>
<u>CLE15_{R50}</u>	<u>1.73</u>	<u>27.70</u>	<u>37.00</u>	<u>0.34</u>
<u>H80_{R64}</u>	<u>-5.67</u>	<u>17.90</u>	<u>23.18</u>	<u>0.14</u>
<u>D87_{R64}</u>	<u>-0.32</u>	<u>18.69</u>	<u>23.92</u>	<u>0.11</u>
<u>W06_{R64}</u>	<u>18.74</u>	<u>21.66</u>	<u>25.24</u>	<u>0.51</u>
<u>E11_{R64}</u>	<u>0.59</u>	<u>17.86</u>	<u>22.98</u>	<u>0.19</u>
<u>F13_{R64}</u>	<u>-14.41</u>	<u>19.89</u>	<u>25.70</u>	<u>0.12</u>
<u>CLE15_{R64}</u>	<u>1.31</u>	<u>18.27</u>	<u>23.54</u>	<u>0.15</u>

426

427

Table 4: Similar to Table 2, but for R_{34} , R_{50} and R_{64} .

	<u>Optimal profile</u>	<u>ME (km)</u>	<u>MAE (km)</u>	<u>RMSE (km)</u>	<u>CE</u>
<u>WP_{R34}</u>	<u>W06</u>	<u>-24.79</u>	<u>46.75</u>	<u>64.54</u>	<u>0.89</u>
<u>WP_{R50}</u>	<u>W06</u>	<u>-14.60</u>	<u>26.00</u>	<u>33.27</u>	<u>0.82</u>
<u>WP_{R64}</u>	<u>W06</u>	<u>-14.14</u>	<u>18.28</u>	<u>22.71</u>	<u>0.78</u>
<u>NA_{R34}</u>	<u>CLE15</u>	<u>-25.19</u>	<u>53.00</u>	<u>78.77</u>	<u>0.87</u>
<u>NA_{R50}</u>	<u>W06</u>	<u>-11.58</u>	<u>32.71</u>	<u>57.39</u>	<u>0.84</u>
<u>NA_{R64}</u>	<u>W06</u>	<u>2.67</u>	<u>18.52</u>	<u>30.37</u>	<u>0.87</u>
<u>NI_{R34}</u>	<u>W06</u>	<u>-23.19</u>	<u>31.19</u>	<u>41.59</u>	<u>0.74</u>
<u>NI_{R50}</u>	<u>W06</u>	<u>-14.66</u>	<u>20.49</u>	<u>25.69</u>	<u>0.63</u>
<u>NI_{R64}</u>	<u>W06</u>	<u>-11.63</u>	<u>16.62</u>	<u>21.17</u>	<u>0.62</u>
<u>SI_{R34}</u>	<u>W06</u>	<u>3.57</u>	<u>45.71</u>	<u>56.68</u>	<u>0.74</u>
<u>SI_{R50}</u>	<u>W06</u>	<u>14.35</u>	<u>29.69</u>	<u>36.18</u>	<u>0.46</u>
<u>SI_{R64}</u>	<u>W06</u>	<u>9.68</u>	<u>18.54</u>	<u>21.57</u>	<u>0.43</u>
<u>SP_{R34}</u>	<u>W06</u>	<u>-5.00</u>	<u>33.51</u>	<u>46.25</u>	<u>0.83</u>
<u>SP_{R50}</u>	<u>W06</u>	<u>11.75</u>	<u>21.53</u>	<u>27.25</u>	<u>0.77</u>

SP_{R64}	W06	12.75	15.60	18.56	0.77
EP_{R34}	W06	32.25	44.43	51.31	0.81
EP_{R50}	W06	27.19	31.77	36.61	0.68
EP_{R64}	W06	18.74	21.66	25.24	0.51

428 ~~We use t~~The ERA5 dataset ~~was is used~~ to derive parameters characterizing TC intensity and size in creating the TC
429 reconstruction dataset. Then, ~~we subject these parameters to a machine learning algorithm to produce more accurate data~~
430 ~~these parameters were are subjected to a machine learning algorithm to produce more accurate data.~~ ~~Notably, we~~
431 ~~acknowledge that the TC intensity and size reconstructions developed in this study may be influenced by the limitations~~
432 ~~and uncertainties inherent in the IBTrACS and ERA5 datasets.~~ ~~Notably, the TC intensity and size reconstructions~~
433 ~~developed in this study may be influenced by limitations and uncertainties inherent to the IBTrACS and ERA5 datasets.~~
434 The RF models ~~were are~~ unable to differentiate between landfall and offshore TCs due to the limited data available
435 concerning landfall TCs in the IBTrACS dataset, which result~~sed~~ in higher V_{max} and lower R_{max} values for landfall
436 TCs. ~~Therefore, w~~When employing this dataset for the purpose of examining the characteristics and impacts of TCs
437 ~~during their landfall, it is possible to, there exists a propensity to overestimate their intensity while underestimating the~~
438 ~~scope of their influence~~the extent of their influence. Additionally, ~~we estimate~~ R_{34} , R_{50} and R_{64} ~~were are estimated~~
439 using wind profile models rather than RF models due to the paucity of relevant data, which result~~sed~~ in a lower level of
440 accuracy than for these TC characteristics. Moreover, there ~~was is~~ some dependency between the reconstructed and
441 IBTrACS-derived R_{max} values, likely due to the insufficient spatial resolution of the ERA5 dataset.
442 ~~Finally~~Finally, ~~Besides,~~ TC positions in the IBTrACS data exhibit~~ed~~ some degree of inaccuracy during the pre-satellite
443 time period. ~~Therefore, when assessing the impacts of TCs with using this dataset, e.g., TC risk assessment, it is crucial~~
444 ~~to validate the finding~~results through a combination of observations from meteorological stations, buoys, and other
445 ~~relevant observational mean~~methods. Notwithstanding these limitations, the TC reconstruction dataset exhibit~~sed~~ a
446 markedly high degree of accuracy and extensive spatiotemporal coverage. Basic information on the reconstructed TC
447 data is presented in Table 57.

Table 57: Basic information on the number of recorded tropical cyclone characteristics from 1959 to 2022 recorded in reconstructed data.

Basin	V_{max}	P_{min}	R_{max}	R_{34}	R_{50}	R_{64}
Western Pacific	152208	152208	152208	127668	39659	24302
North Atlantic	55608	55608	55608	31829	19106	11719
North Indian	24047	24047	24047	4614	1840	1039
South Indian	86606	86606	86606	35768	18500	10395
South Pacific	45112	45112	45112	23312	10547	5454
Eastern Pacific	59112	59112	59112	33772	19214	13026
Global	422693	422693	422693	256963	108866	65935

5. Data and Code availability

All data have been published in the form of CSV files, and are made publicly available through Zenodo repository with the address: <https://doi.org/10.5281/zenodo.13919874>~~https://doi.org/10.5281/zenodo.12740372~~ (Xu et al., 2024). ERA5 data can be publicly accessible at <https://doi.org/10.24381/cds.bd0915c6> (Hersbach et al., 2023a) and <https://doi.org/10.24381/cds.adbb2d47> (Hersbach et al., 2023b). IBTrACS data is accessible at <https://doi.org/10.25921/82ty-9e16> (Gahtan et al., 2024). The processing codes can be made available upon request to the corresponding author. This study provides a detailed description of the TC size and intensity reconstruction dataset, which includes the maximum sustained wind speed, the radius of maximum wind speed, the minimum central pressure and the radii to locations with sustained wind speeds of 34, 50, and 64 knots during 1959–2022.

6. Conclusion

The considerable number of unrecorded TC characteristics in the IBTrACS dataset and large biases inherent in the ERA5 dataset ~~prompted~~ us to generate a long-term TC reconstruction dataset. We constructed the dataset by integrating TC characteristics from the IBTrACS and ERA5 datasets using RF-based models, an empirical wind–pressure relationship, and six wind profiles for the period 1959–2022. The TC reconstruction dataset is approximately 3–4 times larger than the IBTrACS dataset in terms of data points per characteristic, with much higher data accuracy than shown for ERA5-derived results.

~~We examine~~ six TC characteristics ~~were are examined~~ to evaluate the reconstructed dataset. A comparison of maximum sustained wind speeds between the IBTrACS and reconstructed TC datasets ~~revealed~~ that the latter underestimated

468 observational data by approximately 2.82 m/s, which is a considerably smaller bias than that shown by the ERA5 dataset (16.73
469 m/s) on a global scale. For the radius of the maximum wind speed (R_{max}), the mean error and RMSE decreased markedly, from
470 -41.64 and 67.66 km (IBTrACS R_{max} - ERA5 R_{max}) to 1.37 and 22.19 km (IBTrACS R_{max} - reconstructed R_{max}),
471 respectively. In addition, the correlation coefficient for R_{max} between the IBTrACS and ERA5 datasets was 0.44, which
472 increased to 0.94 between the IBTrACS and TC reconstruction datasets. The mean bias in minimum central pressure between
473 the IBTrACS and reconstructed TC datasets was <3% in most basins. We use six wind profile models to
474 compute the radii to locations with sustained wind speeds of 34, 50, and 64 knots (R_{34} , R_{50} , and R_{64}), and the selected wind
475 profile models (CLE15 for R_{34} in the North Atlantic, W06 for others) showed good estimates for TC outer sizes, with
476 correlation coefficients > 0.75 for three outer size metrics in most basins. Overall, the TC reconstruction dataset agreed
477 closely with the IBTrACS data in terms of TC intensity and size.

478 In conclusion, the TC reconstruction dataset may prove invaluable for advancing our understanding of TC climatology,
479 thereby facilitating risk assessments and defenses against TC-related disasters. The future availability of reanalysis data with
480 finer spatial resolution and longer temporal coverage, such as the in-progress ERA6, will facilitate the creation of more accurate
481 TC reconstructions with longer time spans using the methods presented in this study.

482
483 **Author Contributions.** ZX, JG and GZ wrote the first draft of the manuscript. ZX, JG and YY developed the model code and
484 conducted scientific analyses. All authors contributed to the writing and the editing of the manuscript.

485 **Competing interests.** The contact author has declared that none of the authors has any competing interests.

486 **Acknowledgements.** This work was financially supported by the National Natural Science Foundation of China
487 (NSFC42205040 and NSFC42205170), and Youth Innovation Team of China Meteorological Administration (No.
488 CMA2024QN14).

489

490 **References**

- 491 Atkinson G D, and Holliday C R. Tropical cyclone minimum sea level pressure/maximum sustained wind relationship for the
492 western North Pacific. *Monthly Weather Review*, 1977, 105(4): 421-427. [https://doi.org/10.1175/1520-0493\(1977\)105<0421:TCMSLP>2.0.CO;2](https://doi.org/10.1175/1520-0493(1977)105<0421:TCMSLP>2.0.CO;2)
493
- 494 Bell B, Hersbach H, Berrisford P, Dahlgren P, Horányi A, ..., and Thépaut J N. The ERA5 global reanalysis: Preliminary
495 extension to 1950. *Quarterly Journal of the Royal Meteorological Society*, 2021, 147(741): 4186-4227.
496 <https://doi.org/10.1002/qj.4174>
- 497 Bian G F, Nie G Z, and Qiu X. How well is outer tropical cyclone size represented in the ERA5 reanalysis dataset?.
498 *Atmospheric Research*, 2021, 249: 105339. <https://doi.org/10.1016/j.atmosres.2020.105339>
- 499 Bloemendaal N, Haigh I D, de Moel H, Muis S, Haarsma R J, and Aerts J C. Generation of a global synthetic tropical cyclone
500 hazard dataset using STORM. *Scientific data*, 2020, 7(1): 40. <https://doi.org/10.1038/s41597-020-0381-2>
- 501 Breiman L. Random forests. *Machine learning*, 2001, 45: 5-32. <https://doi.org/10.1023/A:1010933404324>
- 502 Casas E G, Tao D, and Bell M M. An intensity and size phase space for tropical cyclone structure and evolution. *Journal of*
503 *Geophysical Research: Atmospheres*, 2023, 128(4): e2022JD037089. <https://doi.org/10.1029/2022JD037089>
- 504 Chavas D R, Lin N, and Emanuel K. A model for the complete radial structure of the tropical cyclone wind field. Part I:
505 Comparison with observed structure. *Journal of the Atmospheric Sciences*, 2015, 72(9): 3647-3662.
506 <https://doi.org/10.1175/JAS-D-15-0014.1>
- 507 Chavas D R, Reed K A, and Knaff J A. Physical understanding of the tropical cyclone wind-pressure relationship. *Nature*
508 *communications*, 2017, 8(1): 1360. <https://doi.org/10.1038/s41467-017-01546-9>
- 509 Chavas D R, and Vigh J. QSCAT-R: The QuikSCAT tropical cyclone radial structure dataset. NCAR Tech. Note TN-5131STR,
510 2014.
- 511 Chu P S. ENSO and tropical cyclone activity. *Hurricanes and typhoons: Past, present, and potential*, 2004, 297: 332.
512 <https://www.soest.hawaii.edu/MET/Hsco/publications/2004.2.pdf>
- 513 [CREED: 2023 Disasters in Numbers: A Significant Year of Disaster Impact – Université catholique de Louvain \(UCL\) – CREED,
514 Brussels, Belgium, available at: \[www.emdat.be\]\(http://www.emdat.be\), 2023](https://www.emdat.be/publications/2023/03/01/cred-2023-disasters-in-numbers-a-significant-year-of-disaster-impact-universite-catholique-de-louvain-ucl-cred-brussels-belgium-available-at-www-emdat-be-2023)
- 515 DeMaria M. Tropical cyclone track prediction with a barotropic spectral model. *Monthly weather review*, 1987, 115(10): 2346-
516 2357. [https://doi.org/10.1175/1520-0493\(1987\)115<2346:TCTPWA>2.0.CO;2](https://doi.org/10.1175/1520-0493(1987)115<2346:TCTPWA>2.0.CO;2)
- 517 Demuth J L, DeMaria M, and Knaff J A. Improvement of Advanced Microwave Sounding Unit tropical cyclone intensity and
518 size estimation algorithms. *Journal of applied meteorology and climatology*, 2006, 45(11): 1573-1581.
519 <https://doi.org/10.1175/JAM2429.1>
- 520 Dulac W, Cattiaux J, Chauvin F, Bourdin S, and Fromang S. Assessing the representation of tropical cyclones in ERA5 with
521 the CNRM tracker. *Climate Dynamics*, 2024, 62(1), 223-238. <https://doi.org/10.1007/s00382-023-06902-8>
- 522 Emanuel K, and Rotunno R. Self-stratification of tropical cyclone outflow. Part I: Implications for storm structure. *Journal of*
523 *the Atmospheric Sciences*, 2011, 68(10): 2236-2249. <https://doi.org/10.1175/JAS-D-10-05024.1>
- 524 Eusebi R, Vecchi G A, Lai C Y, et al. Realistic tropical cyclone wind and pressure fields can be reconstructed from sparse data
525 using deep learning. *Communications Earth & Environment*, 2024, 5(1): 8. <https://doi.org/10.1038/s43247-023-01144-2>
526 2

527 Frisius T, Schönemann D, and Vigh J. The impact of gradient wind imbalance on potential intensity of tropical cyclones in an
528 unbalanced slab boundary layer model. *Journal of the Atmospheric Sciences*, 2013, 70(7): 1874-1890.
529 <https://doi.org/10.1175/JAS-D-12-0160.1>

530 Gahtan J, K R Knapp, C J Schreck, H J Diamond, J P Kossin and M C Kruk. International Best Track Archive for Climate
531 Stewardship (IBTrACS) Project, Version 4r01. NOAA National Centers for Environmental Information, 2024.
532 <https://doi.org/10.25921/82ty-9e16>

533 Geiger T, Frieler K, and Bresch D N. A global historical data set of tropical cyclone exposure (TCE-DAT). *Earth System*
534 *Science Data*, 2018, 10(1): 185-194. <https://doi.org/10.5194/essd-10-185-2018>

535 ~~[CREDGuha Sapid, D. EM DAT: 2023 Disasters in Numbers: A Significant Year of Disaster ImpactThe Emergency](#)~~
536 ~~[Events Database—Université catholique de Louvain \(UCL\)—CRED, Brussels, Belgium, available at:](#)~~
537 ~~www.emdat.be, 20172023~~

538 Gori A, Lin N, Schenkel B, and Chavas D. North Atlantic Tropical Cyclone Size and Storm Surge Reconstructions From
539 1950 - Present. *Journal of Geophysical Research: Atmospheres*, 2023, 128(5): e2022JD037312.
540 <https://doi.org/10.1029/2022JD037312>

541 Gualdi S, Scoccimarro E, Navarra A. Changes in tropical cyclone activity due to global warming: Results from a high-
542 resolution coupled general circulation model. *Journal of climate*, 2008, 21(20): 5204-5228.
543 <https://doi.org/10.1175/2008JCLI1921.1>

544 Guo J, Zhang J, Chen T, Bai K, Shao J, Sun Y, ..., and Hu F. A merged continental planetary boundary layer height dataset
545 based on high-resolution radiosonde measurements, ERA5 reanalysis, and GLDAS. *Earth System Science Data, Earth*
546 *System Science Data*, 2024, 16(1): 1-14. <https://doi.org/10.5194/essd-16-1-2024>

547 Gray W M. Global view of the origin of tropical disturbances and storms. *Monthly Weather Review*, 1968, 96(10): 669-700.
548 [https://doi.org/10.1175/1520-0493\(1968\)096<0669:GVOTOO>2.0.CO;2](https://doi.org/10.1175/1520-0493(1968)096<0669:GVOTOO>2.0.CO;2)

549 Harper B. Tropical cyclone parameter estimation in the Australian Region. Systems Engineering Australia Pty Ltd for
550 Woodside Energy Ltd, Perth, 2002, 83(10.13140).

551 Hatsushika H, Tsutsui J, Fiorino M, and Onogi K. Impact of wind profile retrievals on the analysis of tropical cyclones in the
552 JRA-25 reanalysis. *Journal of the Meteorological Society of Japan. Ser. II*, 2006, 84(5): 891-905.
553 <https://doi.org/10.2151/jmsj.84.891>

554 Hersbach H., Bell B., Berrisford P., Biavati G., Horányi A., Muñoz Sabater J., Nicolas J., Peubey C., Radu R., Rozum I.,
555 Schepers D., Simmons A., Soci C., Dee D., Thépaut J-N. ERA5 hourly data on pressure levels from 1940 to present.
556 Copernicus Climate Change Service (C3S) Climate Data Store (CDS), 2023a. <https://doi.org/10.24381/cds.bd0915c6>

557 Hersbach H., Bell B., Berrisford P., Biavati G., Horányi A., Muñoz Sabater J., Nicolas J., Peubey C., Radu R., Rozum I.,
558 Schepers D., Simmons A., Soci C., Dee D. ERA5 hourly data on single levels from 1940 to present. Copernicus Climate
559 Change Service (C3S) Climate Data Store (CDS), 2023b. <https://doi.org/10.24381/cds.adbb2d47>

560 Hill, K. A., and G. M. Lackmann, 2009: Influence of environmental humidity on tropical cyclone size. *Mon. Wea. Rev.*, 137,
561 3294–3315. <https://doi.org/10.1175/2009MWR2679.1>

562 Holland G J. An analytic model of the wind and pressure profiles in hurricanes. *Monthly Weather Review* 108(8):1212-1218.
563 [https://doi.org/10.1175/1520-0493\(1980\)108<1212:AAMOTW>2.0.CO;2](https://doi.org/10.1175/1520-0493(1980)108<1212:AAMOTW>2.0.CO;2)

564 Kistler R, Kalnay E, Collins W, Saha S, White G, Woollen J, ..., and Fiorino M. The NCEP–NCAR 50-year reanalysis: monthly
565 means CD-ROM and documentation. *Bulletin of the American Meteorological society*, 2001, 82(2): 247-268.
566 [https://doi.org/10.1175/1520-0477\(2001\)082<0247:TNNYRM>2.3.CO;2](https://doi.org/10.1175/1520-0477(2001)082<0247:TNNYRM>2.3.CO;2)

567 Kobayashi S, Ota Y, Harada Y, Ebita A., Moriya M, Onoda H, ..., and Takahashi K. The JRA-55 reanalysis: General
568 specifications and basic characteristics. *Journal of the Meteorological Society of Japan. Ser. II*, 2015, 93(1): 5-48.
569 <https://doi.org/10.2151/jmsj.2015-001>

570 Kowaleski A M, and Evans J L. A reformulation of tropical cyclone potential intensity theory incorporating energy production
571 along a radial trajectory. *Monthly Weather Review*, 2016, 144(10): 3569-3578. [https://doi.org/10.1175/MWR-D-15-](https://doi.org/10.1175/MWR-D-15-0383.1)
572 [0383.1](https://doi.org/10.1175/MWR-D-15-0383.1)

573 Li X, Han X, Yang J, Wang J, and Han G. Transfer learning-based generative adversarial network model for tropical cyclone
574 wind speed reconstruction from SAR images. *IEEE Transactions on Geoscience and Remote Sensing*, 2024.
575 10.1109/TGRS.2024.3390392

576 Lin N, and Chavas D. On hurricane parametric wind and applications in storm surge modeling. *Journal of Geophysical*
577 *Research: Atmospheres*, 2012, 117(D9). <https://doi.org/10.1029/2011JD017126>

578 Liu K S, Chan J C L. Size of tropical cyclones as inferred from ERS-1 and ERS-2 data. *Monthly Weather Review*, 1999,
579 127(12): 2992-3001. [https://doi.org/10.1175/1520-0493\(1999\)127<2992:SOTCAI>2.0.CO;2](https://doi.org/10.1175/1520-0493(1999)127<2992:SOTCAI>2.0.CO;2)

580 Magnusson L, Majumdar S, Emerton R, Richardson D, Balmaseda M, and Zsótér E. Tropical cyclone activities at
581 ECMWF. ECMWF, University of Miami, ECMWF Technical Memoranda, 2021.

582

583 [Mo Y, Simard M, and Hall J W. Tropical cyclone risk to global mangrove ecosystems: potential future regional shifts. *Frontiers*
584 *in Ecology and the Environment*, 2023, 21\(6\): 269-274. <https://doi.org/10.1002/fee.2650>](https://doi.org/10.1002/fee.2650)

585 [Pérez-Alarcón A, Sorí R, Fernández-Alvarez J C, Nieto R, and Gimeno L, et al. Comparative climatology of outer tropical
586 cyclone size using radial wind profiles. *Weather and Climate Extremes*, 2021, 33: 100366.
587 <https://doi.org/10.1016/j.wace.2021.100366>](https://doi.org/10.1016/j.wace.2021.100366)

588 Radu R, Toumi R, Phau J. Influence of atmospheric and sea surface temperature on the size of hurricane Catarina. *Quarterly*
589 *Journal of the Royal Meteorological Society*, 2014, 140(682): 1778-1784. <https://doi.org/10.1002/qj.2232>

590 Ren H, Dudhia J, and Li H. The size characteristics and physical explanation for the radius of maximum wind of hurricanes.
591 *Atmospheric Research*, 2022, 277: 106313. <https://doi.org/10.1016/j.atmosres.2022.106313>

592 Schenkel B A, and Hart R E. An examination of tropical cyclone position, intensity, and intensity life cycle within atmospheric
593 reanalysis datasets. *Journal of Climate*, 2012, 25(10): 3453-3475. <https://doi.org/10.1175/2011JCLI4208.1>

594 Schenkel B A, Lin N, and Chavas D. Evaluating outer tropical cyclone size in reanalysis datasets using QuikSCAT data.
595 *Journal of Climate*, 2017, 30(21): 8745-8762. <https://doi.org/10.1175/JCLI-D-17-0122.1>

596 Simpson R H. The hurricane disaster—Potential scale. *Weatherwise*, 1974, 27(4): 169-186.
597 <https://doi.org/10.1080/00431672.1974.9931702>

598 Sun Y, Zhong Z, Ha Y, Wang Y, and Wang X. The dynamic and thermodynamic effects of relative and absolute sea surface
599 temperature on tropical cyclone intensity. *Acta Meteorologica Sinica*, 2013, 27(1): 40-49., [https://10.1007/s13351-013-](https://10.1007/s13351-013-0105-z)
600 [0105-z](https://10.1007/s13351-013-0105-z).

601 Sun Y, Zhong Z, Yi L, Ha Y, and Sun Y. The opposite effects of inner and outer sea surface temperature on tropical cyclone
602 intensity. *Journal of Geophysical Research: Atmospheres*, 2014, 119(5): 2193-2208. <https://10.1002/2013jd021354>

603 [Thompson D T, Keim B D, and Brown V M. Construction of a tropical cyclone size dataset using reanalysis data. *International*
604 *Journal of Climatology*, 2024, 44\(9\): 3028-3053. <https://doi.org/10.1002/joc.8511>](https://doi.org/10.1002/joc.8511)

605 Walsh K J E, McBride J L, Klotzbach P J, Balachandran S, Camargo S J, Holland G, ... and Sugi M. Tropical cyclones and
606 climate change. *Wiley Interdisciplinary Reviews: Climate Change*, 2016, 7(1): 65-89. <https://doi.org/10.1002/wcc.371>

607 Weber H C, Lok C C F, Davidson N E, and Xiao Y. Objective estimation of the radius of the outermost closed isobar in tropical
608 cyclones. *Tropical Cyclone Research and Review*, 2014, 3(1): 1-21. https://doi.org/10.6057/2014TCRR01_01

609 Willoughby H E, Darling R W R, and Rahn M E. Parametric representation of the primary hurricane vortex. Part II: A new
610 family of sectionally continuous profiles. *Monthly weather review*, 2006, 134(4): 1102-1120.
611 <https://doi.org/10.1175/MWR3106.1>

612 Wu L, Zhao H, Wang C, Cao J, and Liang J. Understanding of the effect of climate change on tropical cyclone intensity: A
613 Review. *Advances in Atmospheric Sciences*, 2022, 39(2): 205-221. <https://doi.org/10.1007/s00376-021-1026-x>.

614 [Wright C J. Quantifying the global impact of tropical cyclone - associated gravity waves using HIRDLS, MLS, SABER and
615 IBrACS data. Quarterly Journal of the Royal Meteorological Society, 2019, 145\(724\): 3023-3039.
616 https://doi.org/10.1002/qj.3602](https://doi.org/10.1002/qj.3602)

617 Xu Z, Sun Y, Li T, Zhong Z, Liu J and Ma C. Tropical cyclone size change under ocean warming and associated responses of
618 tropical cyclone destructiveness: idealized experiments. *Journal of Meteorological Research*, 2020, 34(1): 163-175.
619 <https://doi.org/10.1007/s13351-020-8164-4>.

620 Xu Z, Guo J, Zhang G, Ye Y, Zhao H and Chen, H. Global tropical cyclone size and intensity reconstruction dataset for 1959–
621 2022 based on IBrACS and ERA5 data. Zenodo, 2024.
622 <https://doi.org/10.5281/zenodo.1391987410.5281/zenodo.12740372>

623 Yang Q, Lee C Y, Tippett M K, Chavas D R, and Knutson T R. Machine learning–based hurricane wind reconstruction.
624 *Weather and Forecasting*, 2022, 37(4): 477-493. <https://doi.org/10.1175/WAF-D-21-0077.1>

625 Yeasmin A, Chand S, and Sultanova N. Reconstruction of tropical cyclone and depression proxies for the South Pacific since
626 the 1850s. *Weather and Climate Extremes*, 2023, 39: 100543. <https://doi.org/10.1016/j.wace.2022.100543>

627 Zhuo J Y, Tan Z M. A Deep-Learning Reconstruction of Tropical Cyclone Size Metrics 1981–2017: Examining Trends.
628 *Journal of Climate*, 2023, 36(15): 5103-5123. <https://doi.org/10.1175/JCLI-D-22-0714.1>

629 [Zick S E and Matyas C J. Tropical cyclones in the North American Regional Reanalysis: The impact of satellite-derived
630 precipitation over ocean. Journal of Geophysical Research: Atmospheres, 2015, 120\(17\): 8724-8742.
631 https://doi.org/10.1002/2015JD023722](https://doi.org/10.1002/2015JD023722)

632 ~~Magnusson L, Majumdar S, Emerton R, Richardson D, Balmaseda M, ..., and Zsótér E. Tropical cyclone activities at ECMWF.
633 ECMWF, University of Miami. ECMWF Technical Memoranda, 2021.~~